國立臺灣大學電機資訊學院光電工程學研究所

碩士論文

Graduate Institute of Photonics and Optoelectronics

College of Electrical Engineering and Computer Science

National Taiwan University

Master Thesis

從奈米到微米結構設計以達成氮化銦鎵/氮化鎵元件

之高效能光擷取/光萃取

Efficient Light Harvesting/Extraction Schemes Employing Structure Designs from Microscale to Nanoscale for InGaN/GaN Devices

研究生: 何政翰

Cheng-Han Ho

指導教授：何志浩 博士

Advisor:Jr-Hau He, Ph.D.

中華民國 101 年 6 月

June, 2012

國立臺灣大學碩士學位論文
口試委員會審定書

從奈米到微米結構設計以達成氮化銦鎵/
氮化鎵元件之高效能光擷取/光萃取
Efficient Light Harvesting/Extraction Schemes
Employing Structure Designs from Microscale to
Nanoscale for InGaN/GaN Devices

本論文係何政翰君（學號 R99941049）在國立臺灣大學光電工程學研究所完成之碩士學位論文，於民國 101 年 6 月 27 日承下列考試委員審查通過及口試及格，特此證明

口試委員：

何志浩 （指導教授）

許進恭

黃建璋

所長 林清富

致謝

在研究所短短兩年時間，能完成這篇碩士論文及其餘的研究成果，我要特別感謝我的指導教授何志浩老師、賴昆佑老師及林冠中學長，也要感謝實驗室的每一位成員對我的幫助與給我的建議，這段時間能有你們的陪伴真的很好，不論是課業、研究實驗及日常生活上，大家彼此互助，有困處也不吝於給予幫助，使我們實驗室像個溫暖的家，謝謝大家。另外，也要感謝所有的口試委員，能特地撥空前來給予我指導，使本篇論文內容更加地完整。

回想剛進研究所的前半年，實驗上遭遇了種種的不順利及不愉快，多虧了實驗室政營學長、伯康學長的建議及鼓勵，才使我的實驗漸漸步上軌道，一步步的從做實驗、模擬到寫出論文，也感謝老師平時在研究之外，教導我們做人處事應有的態度及觀念，對我受益良多，也確實讓我學到了課本以外學不到的東西，我想老師、學長教給我的想法觀念，應該會一輩子在我的生活、工作裡時時提醒、督促著我，讓我不斷進步、成長。研究所的這兩年，我覺得是我求學生涯裡過得最有價值的兩年，最後，感謝並祝福所有曾給予我幫助的老師、同學們。

政翰 謹誌於台大

2012 年 6 月

摘要

在本篇論文中,我們將先討論氮化鎵系的太陽能電池,接著為氮化鎵系的發光二極體,最後是我們的總結。

首先,在氮化銦鎵系的多重量子井太陽能電池上,利用自組裝的銀奈米小球當作蝕刻遮罩,去做反應式離子蝕刻,製做出二氧化矽奈米柱陣列。由於光捕捉效應及折射率的匹配(在空氣及元件間),使此二氧化矽奈米柱陣列可有效地降低元件的表面反射率(從330至570奈米波段)。電池在模擬太陽光源(air mass 1.5G)的照射下,其短路電流明顯提升,而轉換效率可增加 21 %。模擬軟體的分析也進一步証明此表面結構能改善電池的光伏特性。

第二,將太陽能電池的 p 型氮化鎵層製做成微米鐘的結構,也可以顯著的提升其轉化效率達 102 %之多。此微米鐘結構能降低元件表面的反射率,增加電池的光吸收能力,並提升短路電流及填充因子。此經由磊晶直接成長出微米鐘的方法,可有效的改善元件的光伏特性。

第三,二氧化矽奈米柱陣列/p 型氮化鎵微米鐘的分層結構被應用在氮化銦鎵的多層量子井太陽能電池上,以當作光擷取層。同樣以自組裝的銀球當作蝕刻遮罩來做反應式離子蝕刻,來將二氧化矽奈米柱陣列製作於 p 型氮化鎵微米鐘之上。由於此粗糙結構的光捕捉效應以及奈米柱具匹配的折射率,使得介面的菲涅耳反射(Fresnel reflection)能被更有效地降低。具此分層結構的電池表現出優異的光伏特性,能提升短路電流及填充因子,進而使轉換效率增加 1.47 倍。此外,元件光吸收能力的增加與以有限差分時域法(finite-difference time-domain, FDTD)分析的結果相吻合。

最後,我們將此分層結構應用在 LED 上,發現能增加 LED 的出光強度。與表面未經粗化的 LED 相比,在 20mA 注入電流下,微米鐘 LED 出光強度增強 16.7 %,而奈米柱/微米鐘 LED 則增強了 36.8 %之多。此結果歸因於粗化結構能使出射光

散射並提供一等效折射率，來降低元件的內部全反射，進而提高光萃取率。此 LED 出光強度的增加也同樣可由有限差分時域法來分析得到。

IV

Abstract

In this thesis, we will firstly focus on InGaN/GaN solar cells, and secondly we move to GaN/InGaN light emitting diodes. The final is our conclusion.

First, SiO_2 nanorod arrays (NRAs) are fabricated on InGaN-based multiple quantum well (MQW) solar cells using self-assembled Ag nanoparticles as the etching mask and subsequent reactive ion etching. The SiO_2 NRAs effectively suppress the undesired surface reflections over the wavelengths from 330 to 570 nm, which is attributed to the light-trapping effect and the improved mismatch of refractive index at the air/MQW device interface. Under the air mass 1.5 global illumination, the conversion efficiency of the solar cell is enhanced by ~21 % largely due to increased short-circuit current from 0.71 to 0.76 mA/cm^2. The enhanced device performances by the optical absorption improvement are supported by the simulation analysis as well.

Second, InGaN-based multiple quantum well (MQW) solar cells (SCs) employing the p-GaN microdome were demonstrated to significantly boost the conversion efficiency by 102 %. The improvements in short-circuit current density (J_{sc}, from 0.43 to 0.54 mA/cm^2) and fill factor (from 44 % to 72 %) using the p-GaN microdome are attributed to enhanced light absorption due to surface reflection suppression. The concept of microdome directly grown during SC epitaxial growth preserving mechanical robustness and wafer-scale uniformity proves a promising way in promoting the photovoltaic performances of SCs without any additional process.

Third, the hierarchical structure of SiO_2 nanorod arrays/p-GaN microdomes was applied as a light harvesting scheme on InGaN-based multiple quantum well solar

cells. Using self-assembled Ag nanoparticles as the etching mask and subsequent reactive ion etching, SiO_2 NRAs were fabricated upon the p-GaN microdomes. Due to the light trapping effect of the roughness and the improved match of refractive index by SiO_2 nanorod arrays, the undesired Fresnel reflections are effectively suppressed. Cells with the hierarchical surfaces exhibit excellent photovoltaic performances including enhanced short-circuit current densities and fill factor, and the measured conversion efficiency is enhanced by 1.47-fold. The improved light absorption in device is consistent with the finite-difference time-domain analysis.

Finally, we report the enhanced light extraction efficiency of the hierarchical structure, SiO_2 nanorods/p-GaN microdomes, fabricating on InGaN/GaN LEDs. Compared with conventional flat LEDs, the light output intensity of bare microdome LED presents an improvement of 16.7 % at 20 mA, yet it boosts to 36.8 % for SiO_2 NRA/p-GaN microdome LED. The results are attributed to the scattering effect and the effective refraction indexes of the textured structures that reduce the total internal reflection, contributing to the most light extraction. The enhanced optical performances are supported by the improved light output power calculated by finite-difference time-domain analysis.

Keywords: Solar cell (SC), InGaN/GaN, Reactive ion etching (RIE), Nanorod, Antireflection, Light harvesting, Microdome, Light-emitting diode (LED), Internal/External quantum efficiency (IQE/EQE), Light extraction efficiency.

List of Contents

List of Figures and Tables

Chapter 3

Chapter 4

Chapter 5

Chapter 6

driving current, respectively.

Chapter 1   Introduction

Recently, since much attention has been paid to the issue of energy shortage, III-V based optoelectronic devices, such as solar cells (SCs) and light-emitting diodes (LEDs), gradually become the promising elements with the remarkable potential of energy reserve. Extensive researches have been devoted to the development of InGaN-based SCs and LEDs. The light-harvesting and light-extracting layers are crucial for eliminating optical loss for optical elements, and have many practical applications to SCs and LEDs.

In this thesis, we firstly use an efficient method to have the SiO_2 nanorods to harvest much light. The approach by using process of self-assembled Ag nanopraticles and RIE for the SiO_2 nanorod fabrication is a useful and low cost technique. To further enhance the solar-energy harvesting of SCs, approaches to fabricate antireflection coatings or subwavelength structures with the additional photo-lithography and wet/dry etching processes have been devoted. However, these approaches are relatively complex and may further damage the devices. In this regard, we secondly performed self-assembled p-GaN microdome structure which is directly grown during the epitaxial growth of SCs. This simple and direct fabrication preserves the nanostructured device with mechanical robustness, wafer-scale

uniformity and stability. The microdomed structure improves the device performances by reducing the internal piezoelectric field and increasing the light absorption by light trapping effect. Integrating microdomes with SiO_2 nanorods is supposed to bring about the most energy-harvesting ability for both SC and LED devices, which will be demonstrated in the following contents. This would in turn lead to nitride-based SCs and LEDs with high efficiency. We believe that this approach is of great interest for researchers working in solar cell devices and III-Nitride optoelectronics device technologies.

Chapter 2　Experimental setup

The SEM images were recorded by a JEOL JSM-6500 field emission scanning electron microscope (SEM). The specular reflection spectra were obtained using a standard UV-visible spectrometer (JASCO ARN-733) at the incident angle of 5°. An external quantum efficiency (EQE) measurement was carried out under the monochromatic illumination by a halogen lamp coupled to a monochromator. The current density-voltage (*J-V*) curves of solar cells were measured with a Keithley 4200 source meter under the illumination of air mass 1.5 global solar simulator (100 mW/cm^2). The electrical characteristics ($I-V$ curves) of LEDs were measured with a Keithley 2400 source meter. The electroluminescence (EL) spectrum was measured using an Ocean Optics USB2000 spectrometer.

Chapter 3   An efficient light-harvesting scheme

using SiO₂ nanorods for InGaN MQW solar cells

§ 3-1   Introduction

InGaN-based solar cells have recently drawn much research attention due to many desired photovoltaic (PV) characteristics, including the potential to realize nearly full absorption of solar spectrum, high absorption coefficients, and high mobilities.[1-3] In addition, InGaN alloys have superior radiation resistance, thermal stability, and chemical tolerance.[3] In consideration of the structure design for active regions, multiple quantum wells (MQWs) consisting of the InGaN layers thinner than the critical thickness on GaN not only prevent the formation of undesired crystal defects, but also provide an additional control of light absorption through the quantized energy levels.[4]

A number of methods have been developed to improve the performances of InGaN-based MQW solar cells.[5-8] For example, Ag nanoparticles have been utilized to induce plasmonic resonance on the device surface to enhance light absorption in the InGaN active region.[7] Kuwahara *et al.* reported that the PV performances of InGaN solar cells with supperlattice active layers can be enhanced by optimizing the barrier thickness.[8]

Recently, it is reported that subwavelength nanostructures exhibit superior antireflective (AR) performances to their quarter-wavelength thin-film counterparts.[9,10] It can be clarified by the light trapping effect at short wavelength regions and the effective medium effect at long wavelength regions [11,12], where the nanostructures can be regarded as an effective medium with the effective refractive index (n_{eff}) increasing gradually from air to device surfaces. As the incident light is reflected at different depths in nanostructured layers, the suppression of the reflection over a wide range of wavelengths can occur through destructive interferences among the reflected waves. Periodic subwavelength nanostructures have been fabricated with various techniques, such as the nanosphere lithography [13,14] and the anodic aluminum oxide templates.[15,16] For the practical applications, the interests in the AR nanostructures have been extended to disordered nanostructures using a simple yet scalable method with low cost.[6,9,17,18]

In this study, we fabricated AR SiO_2 nanorod arrays (NRAs) utilizing self-assembled Ag nanoparticles as a mask and reactive ion etching (RIE) techniques with photoresist-free and wafer-scale-uniformity capabilities. SiO_2 NRAs effectively reduce surface reflections over a wide wavelength range and thus InGaN MQW solar cells employing the SiO_2 NRAs generate additional photocurrents, corresponding to the conversion efficiency enhancement of 21 % due to increased short-circuit current

(J_{sc}) from 0.71 to 0.76 mA/cm^2. Simulation results based on finite-difference

time-domain (FDTD) analysis also indicate that the improved device performance is

due to the enhanced optical absorption in the MQW layers upon the application of

SiO$_2$ NRAs. The proposed concept in this study is applicable to other optoelectronic

devices.

§ 3-2   Experiment

The MQW solar cells were grown by metal-organic chemical vapor deposition

on c-plane sapphire substrates. The layer structures consist of nine periods of

intentionally undoped In$_{0.3}$Ga$_{0.7}$N (3 nm)/GaN (17 nm) MQWs, sandwiched by a

2.5-µm n-type and a 0.2-µm p-type GaN layer. In content in the MQWs determined by

x-ray diffraction is around 30 %. Following the growth, transparent Ohmic contacts to

p-GaN were formed with indium tin oxide (ITO) deposited by the electron beam

evaporation. The 1×1 mm^2 diode mesas were then defined by chlorine-based plasma

etching. The contact scheme consists of fingered Ti/Al/Ni/Au metal grids deposited

on the ITO and the n-GaN.

Fig. 3.1 describes the fabrication procedure for SiO$_2$ NRAs. First, the SiO$_2$/Ag

layers with the thickness of 300/15 nm were deposited on the ITO layer of

InGaN/GaN MQW solar cells by the electron beam evaporation [Fig. 3.1(a)]. For

forming Ag nanoparticles, a thermal annealing process was carried out in the furnace

at 270 ℃ for 2 min [Fig. 3.1(b)]. Using these Ag nanoparticles as etching masks, the

SiO$_2$ layer was patterned by the RIE process with CHF$_3$ gas (30 SCCM) and rf power

of 90 W for 9 min [Fig. 3.1(c)]. After removing the remaining Ag nanoparticles by

HNO$_3$, the SiO$_2$ NRAs were obtained, as shown in Fig. 3.1(d). It should be mentioned

that we had controlled Ag thickness from 5 nm to 30 nm, annealing temperatures from

250   to 350   , and annealing times from 1 min to 30 min, which contribute to the

different geometries of self-assembled Ag nanoparticles. Changing etching times from

5 min to 10 min of RIE increased nanorod lengths. After experimental parameter

optimization, the best photovoltaic conversion efficiency of our solar cells devices can

be obtained using 15-nm-thick Ag films combining an annealing process at 270   for

2 min and subsequent RIE process for 9 min.
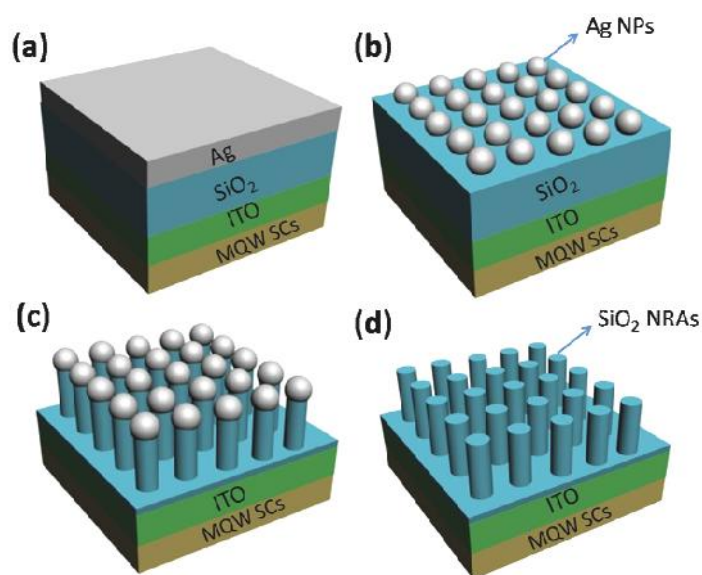
Figure 3.1 Schematic of fabrication procedures for the antireflective nanostructures

7

on InGaN MQW solar cells.

§ 3-3　Results and Discussion

Fig. 3.2(a)-(b) respectively reveal the top-view and 45-degree cross-sectional

images of the fabricated MQW device with SiO_2 NRA surfaces. With Ag

nanoparticles as etching masks, the underlying SiO_2 layer was selectively etched

using a CHF_3 RIE. Because the metal Ag was slowly eroded away during the RIE,

slightly tapered NRAs can be created on the MQW solar cells through prolonged

etching. Using the CHF_3 gas for RIE maintains a smoth surface finish. The average

lengths of the NRAs are around 230 nm, and the diameters are in the range of 50-100

nm, which are controlled by annealing times and temperatures for Ag thin films.

According to Fig. 3.2(a), the area density of the NRAs, defined as the number of

nanorods per unit area, is approximately 1.5×10^{10} cm^{-2}. The coverage of NRAs is

characterized by the fill factor, which is defined by the area ratio of NRAs to the

entire substrate surfaces using the top-view SEM images of Fig. 3.2(a). The fill factor

of the NRA surface is 0.68. The determined fill factor will be used later for

calculating effective refractive index (n_{eff}). It is worth mentioning that the dependence

of AR properties on geometric features for nanorods has been widely studied.[9,19,20] In

particular, it is found that increasing the diameter and the length of the naorods leads

to reduced surface reflectance and improved omnidirectionality. However, it is also found that the over-lengthened nanorods may lead to the degraded J_{sc} despite their lowest reflection, which is attributed to the excessive absorption of the lengthened nanorods.[6] Accordingly, an appropriate length of nanorods is needed for maximizing the J_{sc} enhancement. The robustness of the SiO_2 nanorods can be confirmed during the fabrication process. For the removal of Ag nanoparticles after etching, the SiO_2 nanorods were immersed in 70 % HNO_3 solvent at 40 ℃－50 ℃ for a few minutes. Fig. 3.2 shows that the geometries of the overall NRAs are still well preserved after HNO_3 treatment. These results indicate that the rod-like nanostructure can be fabricated with controllable manner and good yield for achieving low-cost solar devices.
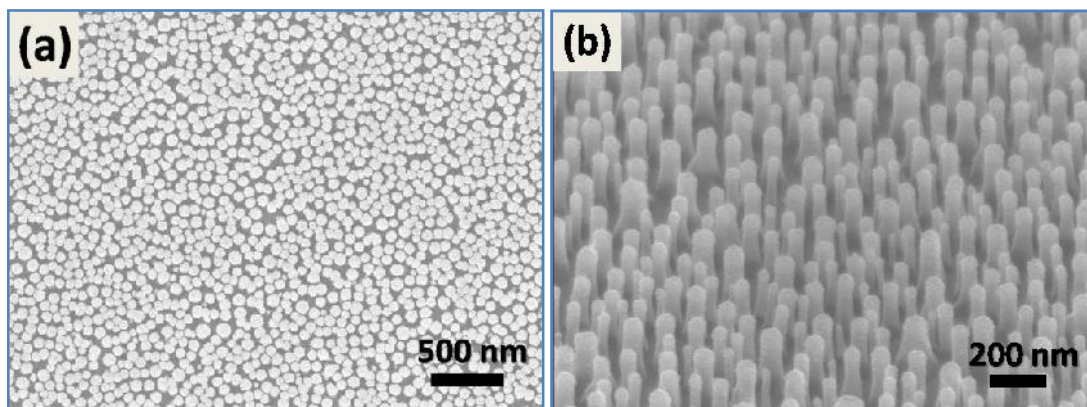
Figure 3.2 (a) Top-view and (b) 45-degree tilted-view SEM images of the SiO_2 NRAs.

Fig. 3.3 is the specular reflection spectra with the wavelengths ranging from 330 to 570 nm. The surface reflectance of the SiO_2 NRA surface is much lower than that on the bare surface for the entire studied wavelengths. The significantly low reflectance at 330-450 nm is particularly important to the efficiency enhancement of the MQW solar cell, which will be shown in the EQE measurements later. The suppressed reflection by NRA structures is attributed to several effects. As the incident wavelength is much higher than the geometric size of NRAs at the long wavelength region, the reduced reflectance can be explained by the effective medium theory. Due to the subwavelength dimensions and the refractive index (around 1.56 at 400 nm) of SiO_2 [21], the SiO_2 NRAs behave like an effective medium with the n_{eff} between the refractive indices of air (~1) and ITO (~2.3) layer. n_{eff} of the NRAs can be estimated by the equation [22]:

$$n_{eff} = \{ f n_{SiO_2}^q + [1 - f n_{air}^q]\}^{1/q} \qquad (1)$$

where q is 2/3, n_{SiO_2} and n_{air} are respectively the refractive indices of SiO_2 and air, and f is the fill factor. The calculated n_{eff} is 1.37 with f = 0.68. Such low n_{eff} is rarely found in natural materials, but is of great importance to achieve broadband AR at the air/device interface. For the short incident wavelength region, the gaps between NRAs lead to the light trapping effect. As the light impinges on the nanostructrued surface, it diffracts to several beams with different diffraction angles, and then re-bounces

between NRAs until the light propagates into MQW regions at a high angle from the

normal, which increases the opportunity of optical absorption by the MQWs due to

the increase of light propagation paths in MQW regions. This speculation will be

further demonstrated by PV measurements and simulations later. We note that the

subwavelength nanostructures result in the suppressed reflectance not only over a

wide range of wavelengths, but also a wide range of incident angles, which can be

clarified by the effective medium theory and the light trapping effect.[23-25]
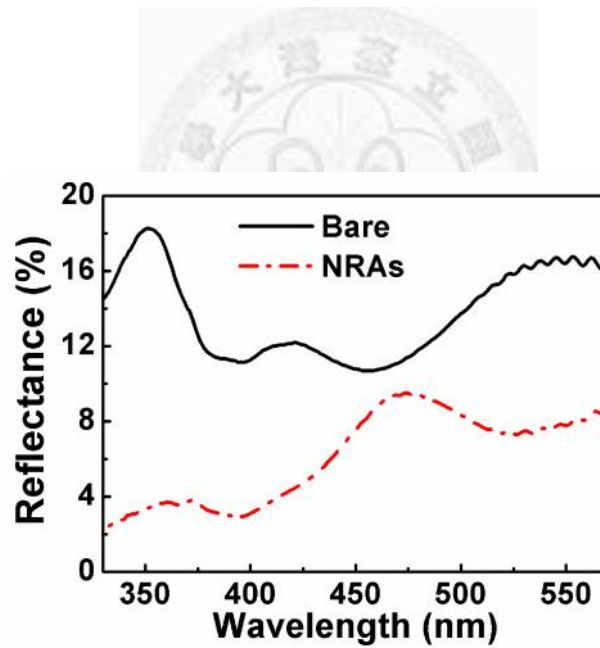
Figure 3.3 Specular reflectance measured on the MQW solar cells with bare and SiO_2
NRA surfaces.

In order to reveal the light propagation across the interfaces, the distributions of electromagnetic fields within the device structures were simulated by FDTD analysis. We modeled the devices with bare and SiO_2 NRA surfaces. Fig. 3.4(a)-(b) visualize the time-averaged TE-polarized electric field intensity distributions, $|E_y|$, for the MQW solar cells with two surface conditions at 380 nm as considering n and k of all materials.[26] All of the calculated values are normalized to the ones of the excitation source. It can be seen that the field intensities inside the InGaN MQW region are enhanced with SiO_2 NRAs. In the inset of Fig. 3.4(b), where the region of SiO_2 NRAs is enlarged, one can see strong field intensity between nanorods, indicating that the nanorods behave as effective scattering centers. The strong scattering within the NRAs therefore prevents the incident waves bouncing back to the air and prolongs the optical path, giving rise to the light-trapping effect. Fig. 3.4(c) shows the normalized optical power, integrated over the MQW region, as a function of times for bare and NRA surfaces. The steady-state power values for the cells with bare and NRA surfaces are 0.744 and 0.824, respectively. The results indicate that the NRAs increase the number of the photons reaching the MQW region, which benefits the conversion efficiency of the MQW solar cell.
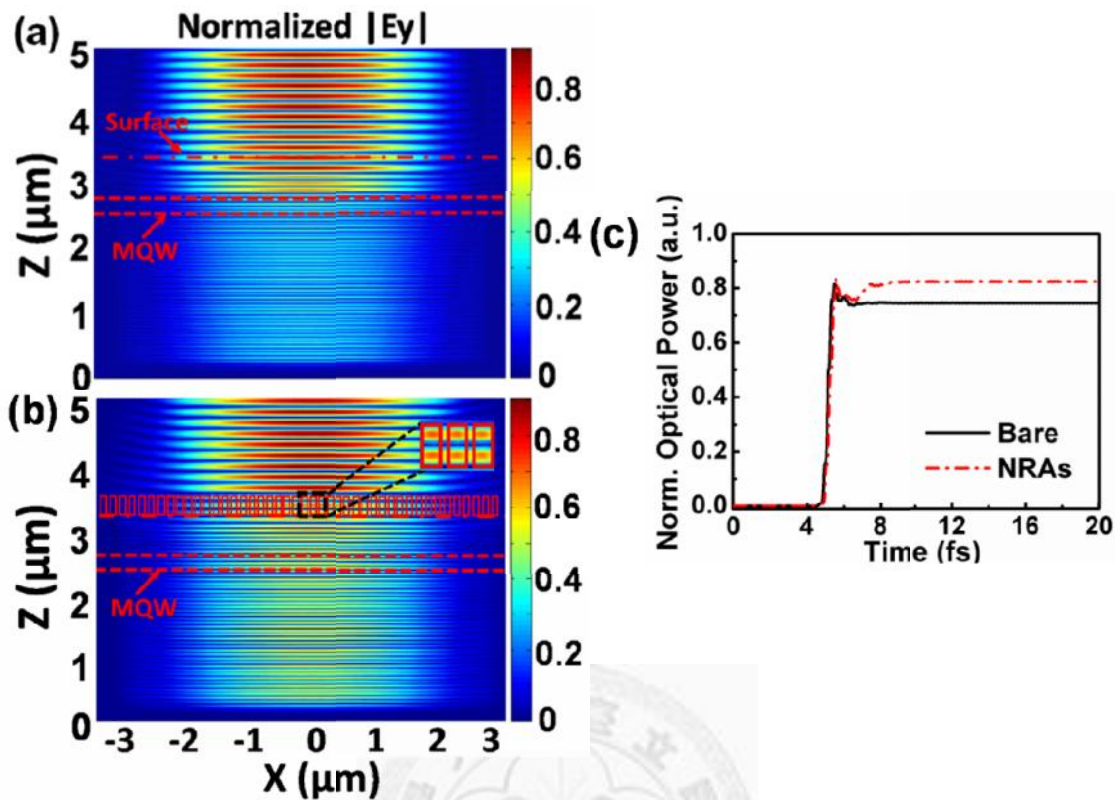
Figure 3.4 Time-averaged, normalized TE electric field distribution, |*E*y|, simulated by FDTD analysis for the MQW solar cells with (a) bare and (b) SiO$_2$ NRA surfaces with a 380-nm incident light. (c) Normalized optical power, integrated over the MQW region, as a function of times for two kinds of solar cells.

Fig. 3.5(a) presents the spectra of the EQE for the MQW solar cells with two kinds of surface conditions, showing the influence of the light-harvesting SiO$_2$ NRAs on PV performances. The EQE for MQW solar cells with SiO$_2$ NRAs is improved at 370-440 nm, which agrees with the reduced reflectance seen in Fig. 3.3. Fig. 3.5(b) shows the *J-V* curves of the two kinds of solar cells. The PV data summarized from

the *J-V* curve is listed in Table 3.1. The agreement between the results in Fig. 3.3, Fig.

3.4, and Fig. 3.5 indicates that the light-harvesting SiO_2 NRAs increase the optical

transmission and light propagation paths through the device surface, and hence

enhance the light absorption in the MQW region, giving rise to the additional

photocurrent of the MQW devices with NRA surfaces. The enhanced J_{sc} hence boosts

the conversion efficiency from 0.37 % to 0.45 %, which is an efficiency improvement

of ~21 %.
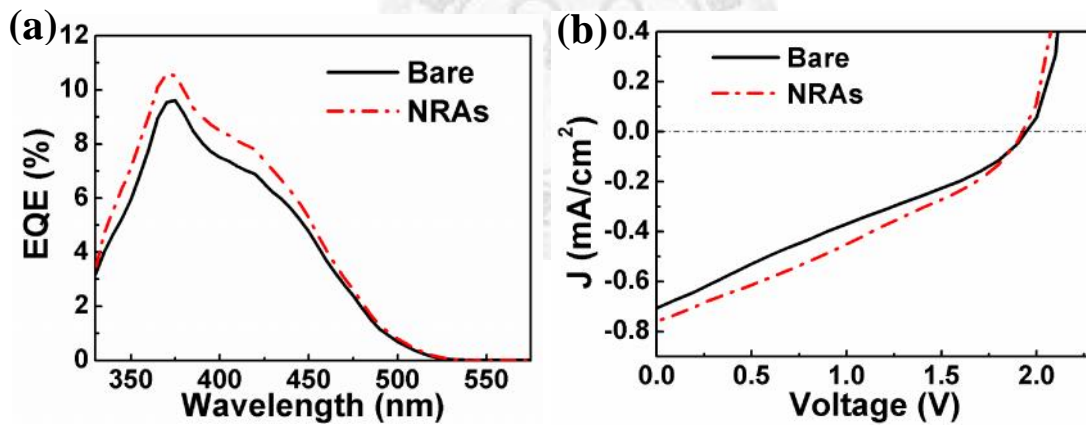
Figure 3.5 (a) EQEs and (b) *J–V* characteristics measured on the MQW solar cells

with bare and SiO_2 NRA surfaces.

Table 3.1 Device characteristics of the MQW solar cells with bare and NRAs surfaces. Note that FF stands for the fill factor of solar cells, which is defined as the ratio of the actual maximum obtainable power, to the product of J_{sc} and open circuit voltage (V_{oc}).

AR Layers	J_{sc} (mA/cm^2)	V_{oc} (V)	FF (%)	(%)
Bare	0.71	1.95	27.28	0.37
SiO$_2$ NARs	0.76	1.93	31.04	0.45

§ 3-4 Summary

Using self-assembled Ag nanoparticles as an etching mask and RIE method, we successfully fabricated low-cost light-trapping SiO$_2$ NRAs to improve the optical absorption of InGaN MQW solar cells. The light-trapping SiO$_2$ NRA layer increases the EQE of the solar cell mostly at 370-440 nm, corresponding to the improvement of conversion efficiency by up to ~21 %. The superior AR performance of the SiO$_2$ NRAs is attributed to the subwavelength dimensions and the nanorod-structured geometry, effectively suppressing the surface reflection at the wavelengths from 330–570 nm via the light trapping effect and the graded n_{eff}, which have been demonstrated by PV measurements and simulations. Presented concepts and manufacturing techniques for light-harvesting nanostructures would be a viable way to boost the efficiency for a variety of PV devices.

§ 3-5　References

[1]　K. Y. Lai, G. J. Lin, Y.-L. Lai, Y. F. Chen, J. H. He, Effect of indium fluctuation on the photovoltaic characteristics of InGaN/GaN multiple quantum well solar cells, Appl. Phys. Lett. 96 (2010) 081103.

[2]　K. Y. Lai, G. J. Lin, Y.-L. Lai, J. H. He, Origin of hot carriers in InGaN-based quantum-well solar cells, IEEE Electron Dev. Lett. 32 (2011) 179–181.

[3]　J. Wu, W. Walukiewicz, K. M. Yu, W. Shan, J. W. Ager, E. E. Haller, H. Lu, W. J. Schaff, W. K. Metzger, S. Kurtz, Superior radiation resistance of $In_{1-x}Ga_xN$ alloys: full-solar-spectrum photovoltaic material system, J. Appl. Phys. 94, (2003) 6477–6482.

[4]　K. W. J. Barnham, G. Duggan, A new approach to high-efficiency multi-band-gap solar cells, J. Appl. Phys. 67 (1990) 3490–3493.

[5]　E. Matioli, C. Neufeld, M. Iza, S. C. Cruz, A. A. Al-Heji, X. Chen, R. M. Farrell, S. Keller, S. DenBaars, U. Mishra, S. Nakamura, J. Speck, C. Weisbuch, High internal and external quantum efficiency InGaN/GaN solar cells, Appl. Phys. Lett. 98 (2011) 021102.

[6]　G. J. Lin, K. Y. Lai, C. A. Lin, Y.-L. Lai, J. H. He, Efficiency enhancement of InGaN-based multiple quantum well solar cells employing antireflective ZnO nanorod arrays, IEEE Electron Dev. Lett. 32 (2011) 1104–1106.

[7]　I. M. Pryce, D. D. Koleske, A. J. Fischer, H. A. Atwater, Plasmonic nanoparticle enhanced photocurrent in GaN/InGaN/GaN quantum well solar cells, Appl. Phys. Lett. 96 (2010) 153501.

[8]　Y. Kuwahara, T. Fujii, T. Sugiyama, D. Iida, Y. Isobe, Y. Fujiyama, Y. Morita, M. Iwaya, T. Takeuchi, S. Kamiyama, I. Akasaki, H. Amano, GaInN-based solar cells using strained-layer GaInN/GaInN superlattice active layer on a

freestanding GaN substrate, Appl. Phys. Express 4 (2011) 021001.

[9]   Y. C. Chao, C. Y. Chen, C. A. Lin, Y. A. Dai, J. H. He, Antireflection effect of ZnO nanorod arrays, J. Mater. Chem. 20 (2010) 8134–8138.

[10] K. Y. Lai, Y. R. Lin, H. P. Wang, J. H. He, Synthesis of anti-reflective and hydrophobic Si nanorod arrays by colloidal lithography and reactive ion etching, Cryst. Eng. Comm. 13 (2011) 1014–1017.

[11] P. Beckman, A. Spizzichno, The scattering of electromagnetic waves from rough surfaces, Pergamon, Oxford, 1963.

[12] P. B. Clapham, M. C. Hutley, Reduction of lens reflexion by the 'moth eye' principle, Nature 244 (1973) 281–282.

[13] L. Li, T. Y. Zhai, H. B. Zeng, X. S. Fang, Y. Bando, D. Golberg, Polystyrene sphere-assisted one-dimensional nanostructure arrays: synthesis and applications, J. Mater. Chem. 21 (2011) 40–56.

[14] X. D. Wang, E. Graugnard, J. S. King, Z. L. Wang, Large-scale fabrication of ordered nanobowl arrays, Nano Lett. 4 (2004) 2223–2226.

[15] Z. Fan, J. C. Ho, Self-assembly of one-dimensional nanomaterials for cost-effective photovoltaics, Int. J. Nanoparticles 4 (2011) 164–183.

[16] Z. Fan, R. Kapadia, P. W. Leu, X. Zhang, Y.-L. Chueh, K. Takei, K. Yu, A. Jamshidi, A. A. Rathore, D. J. Ruebusch, M. Wu, A. Javey, Ordered arrays of dual-diameter nanopillars for maximized optical absorption, Nano Lett. 10 (2010) 3823–3827.

[17] Y. J. Lee, D. S. Ruby, D. W. Peters, B. B. McKenzie, J. W. P. Hsu, ZnO nanostructures as efficient antireflection layers in solar cells, Nano Lett. 8 (2008) 1501–1505.

[18] H. C. Chang, K. Y. Lai, Y. A. Dai, H. H. Wang, C. A. Lin and J. H. He,

Nanowire arrays with controlled structure profiles for maximizing optical collection efficiency, Energy Environ. Sci. 4 (2011) 2863–2869.

[19] Y. R. Lin, H. P. Wang, C. A. Lin and J. H. He, "Surface profile-controlled close-packed Si nanorod arrays for self-cleaning antireflection coatings," J. Appl. Phys. 106 (2009) 114310.

[20] Y. A. Dai, H. J. Chang, K. Y. Lai, C. A. Lin, R. J. Chung, G. R. Lin and J. H. He, "Subwavelength Si nanowire arrays for self-cleaning antireflection coatings," J. Mater. Chem. 20 (2010) 10924–10930.

[21] E. D. Palik, Handbook of Optical Constants of Solids, Academic Press.

[22] D. G. Stavenga, S. Foletti, G. Palasantzas, K. Arikawa, Light on the moth-eye corneal nipple array of butterflies, Proc. R. Soc. B 273 (2006) 661–667.

[23] J. Q. Xi, M. F. Schubert, J. K. Kim, E. F. Schubert, M. Chen, S. Y. Lin, W. Liu, J. A. Smart, Optical thin-film materials with low refractive index for broadband elimination of Fresnel reflection, Nat. Photonics 1 (2007) 176–179.

[24] J. Q. Xi, J. K. Kim, E. F. Schubert, Silica nanorod-array films with very low refractive indices, Nano Lett. 5 (2005) 1385–1387.

[25] S. L. Diedenhofen, G. Vecchi, R. E. Algra, A. Hartsuiker, O. L. Muskens, G. Immink, E. P. A. M. Bakkers, W. L. Vos, J. G. Rivas, Broad-band and omnidirectional antireflection coatings based on semiconductor nanorods, Adv. Mater. 21 (2009) 973–978.

[26] S. Laux, N. Kaiser, A. Zoller, R. Gotzelmann, H. Lauth, H. Bernitzki, Room-temperature deposition of indium tin oxide thin films with plasma ion-assisted evaporation, Thin Solid Films 335 (1998) 1–5.

Chapter 4　Microdome InGaN-Based Multiple Quantum Well Solar Cells

§ 4-1　Introduction

To date, InGaN-based MQW SCs have drawn much research attention due to their favorable photovoltaic (PV) characteristics, including direct and tunable bandgaps covering nearly the entire solar spectrum, high absorption coefficient, high mobility, superior radiation resistance, and additional control of the light absorption through the quantized energy levels.[1,2] Despite these promising characteristics, the conversion efficiencies of InGaN-based MQW SCs are still unsatisfactory. To improve the PV performances of InGaN SCs, much research has been reported.[3-7] In order to mitigate the abrupt change in refractive indices from GaN (or ITO) to air, which blocks a great portion of photons propagating through the air-GaN (or air-ITO) interface,[5] a variety of roughened structures have been employed on the top of InGaN MQW SCs.[3,6,7] Periodic subwavelength structures can be fabricated with various techniques, such as the anodic aluminum oxide templates[8] and the nanosphere lithography.[9,10] For the practical applications, the interests in the subwavelength structures have been extended to disordered structures.[3,11,12] However, the processing complexity and the mechanical robustness of the additional roughened structures on

19

the top of SCs might be a limit to PV applications.

Among various roughened structures, the microdomes (or lens-like microstructures) have been used for increasing the light escape cone in InGaN light-emitting diodes (LEDs),[13-15] resulting in improved light extraction efficiency and engineered far-field.[15] Recently, the use of colloidal microlens arrays had also been implemented for increasing the light extraction in organic light-emitting diodes,[16] as well as improving the light collection in SCs.[17] Additionally, it is found that roughened p-GaN structures in InGaN LEDs can effectively reduce reflectance loss in GaN,[18] and provides an effective way to make p-metal contact deposition without using a filling process with the insulating materials in the air gaps caused by nanostructing/microstructing processes at the device surface, which is required for the axial p-n nanorod devices to form electrical connection.[19] Moreover, the roughened p-GaN also leads to a reduction of piezoelectric field and improved crystal qualities due to the relaxation of in-plane strain.[20,21] Roughening p-GaN is expected to benefit the PV performances of InGaN MQW SCs since numerical studies have demonstrated the detrimental effects of strain-induced piezoelectric polarization, forcing the photocurrent to the opposite direction and thus resulting in low J_{sc} and open-circuit voltage (V_{oc}).[22] Thus, the pursuit of microdome/lens-like structure via roughening p-GaN is of great importance for increasing the critical angle and collection efficiency

in InGaN SCs.

In this study, we realize the p-GaN microdome surfaces with the attempt to boost the conversion efficiencies ( ) of InGaN MQW SCs. Compared with flat p-GaN, the p-GaN microdomes not only generate additional photocurrents (from 0.43 to 0.54 mA/cm^2) by suppressing surface reflections considerably but also exhibit an improved fill factor (from 44 % to 72 %), indicating the strain relaxation and the piezoelectric field reduction. Accordingly, the p-GaN microdome leads to a 102 % enhancement of . The optical enhancement is confirmed using the simulation based on finite-difference time-domain (FDTD) analysis, reflection measurements and external quantum efficiency (EQE) measurements. The internal quantum efficiency (IQE) measurements indicate the possible improvement in photocarrier separation/collection due to the strain relaxation. The concept of the microdome directly grown during SC growth preserving mechanical robustness and wafer-scale uniformity without any additional process represents a viable, promising path toward high-efficiency SCs.

§ 4-2   Experiment

The multiple quantum well (MQW) solar cells (SCs) were grown by metal–organic chemical vapor deposition on c-plane sapphire substrates. The layer structures consist of fifteen periods of intentionally undoped In$_{0.15}$Ga$_{0.85}$N (2.4

nm)/GaN (14 nm) MQWs, sandwiched by a 2.5-µm n-type (Si-doped) and a 0.2-µm

p-type (Mg-doped) GaN layer. The free carrier concentrations for n-type and p-type

GaN are around 2×10^{18} cm^{-3} and 5×10^{17} cm^{-3}, respectively. Ammonia (NH$_3$),

trimethylgallium (TMGa) for n-GaN and p-GaN, triethylgallium for MQWs, and

trimethylindium were used as the precursors. Surface morphologies of p-GaN were

controlled by TMG flows and substrate temperatures during the p-GaN growth. In

device fabrication, ITO was deposited by electron beam evaporation on p-GaN to

form transparent ohmic contacts. The 1×1 mm^2 mesas were then defined by

chlorine-based plasma etching. The contacting scheme consists of fingered

Ti/Al/Ni/Au metal grids with the thicknesses of 20/400/20/2000 nm deposited on the

ITO and the n-GaN.

§ 4-3   Results and Discussion

Surface morphologies of p-GaN were controlled by TMGa flows and substrate

temperatures during the p-GaN growth. For flat p-GaN, TMGa flow rate was 40-50

µmol/min and substrate temperature was in the range of 950-1100 °C. To fabricate the

micro-roughened p-GaN, TMGa flow rate was increased to more than 55 µmol/min

and substrate temperature was decreased to lower than 920 °C. Fig. 4.1 shows

scanning electron microscopy (SEM) images of the MQW SCs with p-GaN

microdome surfaces. The p-GaN microdomes are 530 ± 250 nm in height and the base of microdomes are 600 ± 370 nm in diameter. Fig. 4.2 is the specular reflection spectra obtained on flat and microdome surfaces at the wavelengths ranging from 340 to 600 nm. One can see that the MQW SC with p-GaN microdome surfaces exhibits a low reflectance for all studied wavelengths, demonstrating that surface reflectance can be effectively suppressed by the p-GaN microdomes.
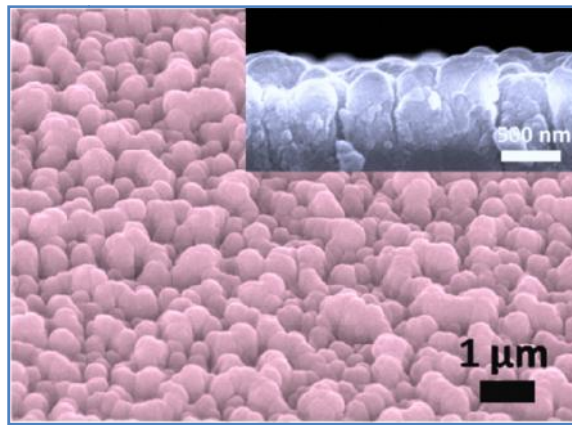
Figure 4.1 45 degree-tilted SEM image of the MQW SCs with p-GaN microdomes. The inset shows the cross-sectional SEM image.
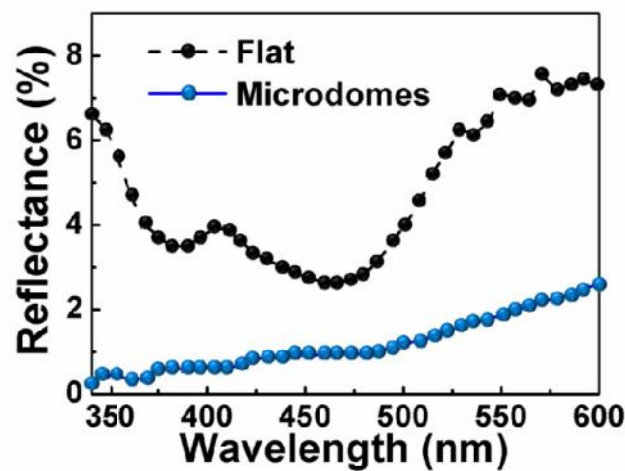
Figure 4.2 Specular reflection measured on the MQW SCs with flat and microdome-like p-GaN surfaces.

For the incident wavelengths comparable or shorter than the geometric sizes of the microdomes, the low reflectance can be caused by the light trapping effect due to severe light scattering. As light impinges on the structured surface, it is diffracted to several beams with different diffraction angles. The diffracted beams re-bounces between the p-GaN microdomes, which prevents the light from escaping back to air, and thus increases the opportunity of optical absorption by the underneath material. It should be mentioned that the light trapping effect results in the suppressed reflectance over not only a wide range of wavelengths but also a wide range of incident angles. [23,24]

In order to reveal the light propagation across the surface structures, the distributions of electromagnetic fields within the device structures were simulated by FDTD analysis. We modeled two kinds of device surfaces: flat p-GaN and p-GaN microdomes. Fig. 4.3 visualizes the time-averaged TE-polarized electric field intensity distributions for the MQW SCs with two surface conditions at the incident wavelength of 400 nm. All of the calculated values in Fig. 4.3 are normalized to those of the excitation source. It can be seen that the light propagating in the MQW region for the SC with p-GaN microdomes is strongly and widely scattered, as compared with the case of flat surface. One can also notice that strong fields are confined within the p-GaN microdomes. The normalized optical power integrated over the MQW

region as a function of times for the SCs with p-GaN flat and microdome surfaces is shown in Fig. 4.3(c). The steady-state power values for the two devices are 0.65 and 0.75, respectively. These results indicate that the roughened p-GaN surface not only helps light propagating across the interfaces but also widens the field distribution within the device by increasing the light scattering on the surface. Strong light scattering by the microdome surface is desired for improving the efficiencies of SCs due to the increase in optical paths, which benefits the light absorption in MQW regions.
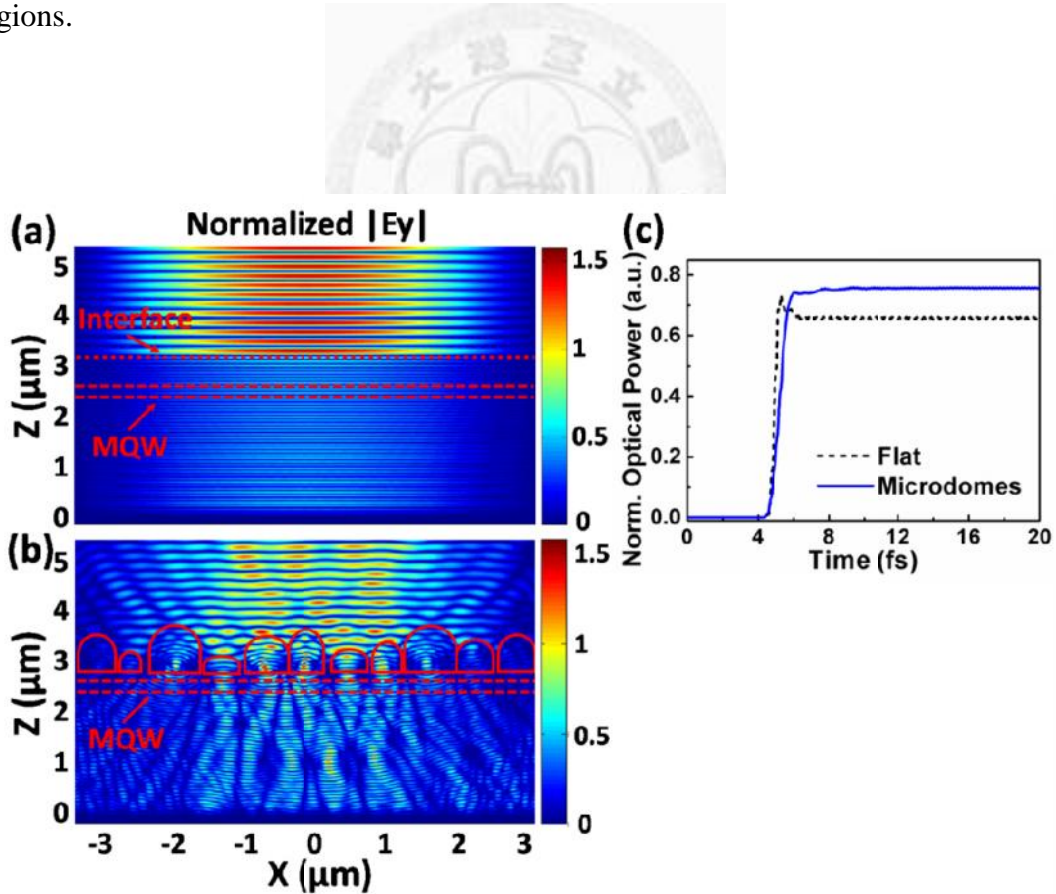
Figure 4.3 Time-averaged and normalized TE electric field distribution simulated by FDTD analysis with two surface structures: (a) flat and (b) p-GaN

microdomes. (c) Normalized optical power, integrated over the MQW region, as a function of times for the two kinds of SCs at 400 nm wavelength.

Fig. 4.4 shows the measured current density–voltage (J–V) curves of the SCs with two kinds of surfaces. PV characteristics obtained by the J–V curves are listed in the inset table of Fig. 4.4. One can clearly see that the microdome surfaces lead to enhanced J_{sc}, which confirms that the microstructured surface enhances light absorption. It is also found that the fill factors are enhanced for the SCs with microdome surfaces suspectedly due to the strain relaxation and the piezoelectric field reduction caused by the roughened structure.[18,20,21] Accordingly, for the SCs with p-GaN microdomes,   is increased from 0.43 % (with flat surface) to 0.87 %, which is an improvement of 102 %. The results prove that the microdomes are effective in boosting the PV performances of the MQW SCs. Note that previous simulation works focusing on wire SCs reported that increasing the wire length could lead to a constant decrease in V_{oc} in spite of increases in   .[25,26] Consequently, a slight decrease in V_{oc} is also observed in the MQW SCs with microdome surfaces. We note that the optimization considerations must be made in future with respect to the geometric parameters of microdome structures due to the inverse behavior of J_{sc} and V_{oc}.[25,26]
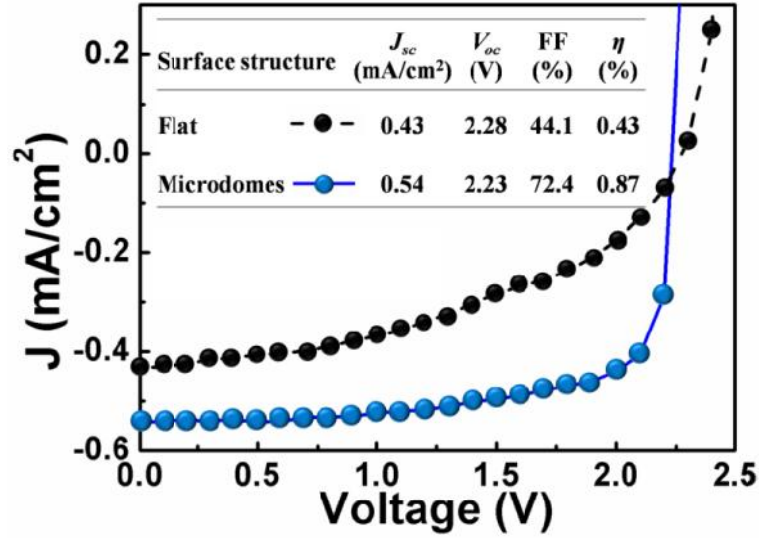
Figure 4.4 *J–V* characteristics measured on the MQW SCs with two kinds of surface structures. The inset table shows PV characteristics of InGaN MQW SCs with two kinds of surface structures. FF is the fill factor of SCs, which is defined as the ratio of the actual maximum obtainable power, to the product of J_{sc} and V_{oc}.

To gain insight into the correlation between J_{sc} enhancement, optical absorption, and carrier separation/collection efficiency in the active layer, EQE and IQE spectra were investigated. Fig. 4.5(a) presents the EQE spectra for the two kinds of SCs, showing the influence of p-GaN microdomes on PV performances. EQEs of the SCs with microdomes are mostly improved in the region of 360–450 nm, which reveals the enhancement in light collection efficiency and agrees with the suppressed reflection on the microdome surface shown in Fig. 4.2. The results also echo with those revealed by FDTD analysis in Fig. 4.3. Since E. Matioli *et al.* had found the

27

possible IQE change in roughened SCs and Wierer *et al.* had demonstrated that SC

performances including IQE can be further improved by optimizing the barrier

thickness of QWs,[4,27] IQE measurements are then taken to evaluate the carrier

separation/collection occurring in the active region. EQE is converted into IQE

through

$$IQE = EQE/abs(\ ) \hspace{4cm} (1)$$

where abs( ) the absorption spectra of the SCs, which is shown in Fig. 4.6. For

absorption spectrum measurements, by measuring reflection and transmission in the

spectral range from 360 to 540 nm, the absorption spectra can be obtained by

subtracting reflection and transmission from unity at every wavelength. Accordingly,

the obtained IQE in Fig. 4.5(b) may point out the possibility of IQE changes due to

p-GaN roughening. The variation in IQE after introducing p-GaN microdomes

indicates the possible change in carrier separation/collection efficiency resulted from

relaxation of in-plane strain and consequent reduction of piezoelectric fields during

p-GaN microdome growth.[22] One should note that the possible inaccuracy in

determining the absorption spectra due to the difference in the surfaces for both SCs

might not enable one to provide accurate IQE comparison data for both devices. For

correctly determining the IQE for both devices, more detailed experiments in

providing conclusive comparison are required in future. In short, the p-GaN

microdome results in the increases in EQE, which are attributed to the suppressed

interface reflection and possibly efficient separation/collection of photocarriers.
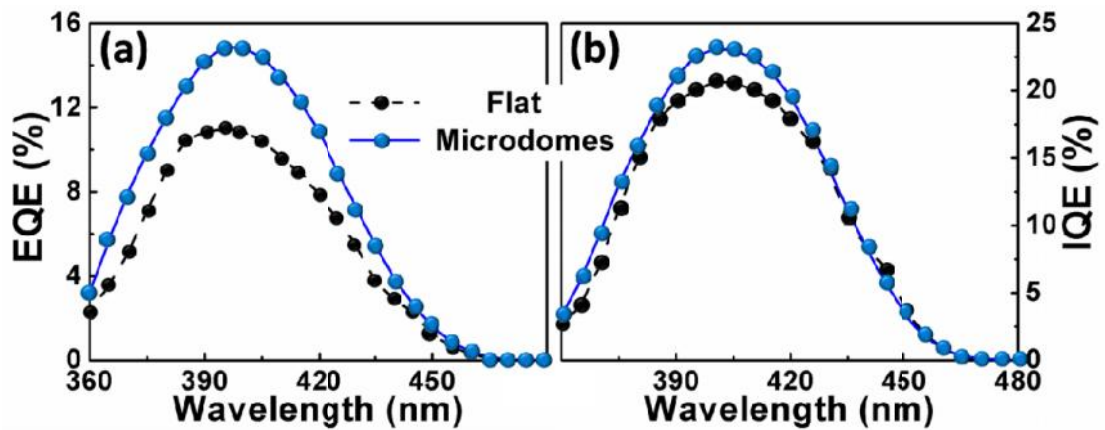
Figure 4.5 (a) EQE curves and (b) IQE curves for the SCs with two kinds of surface
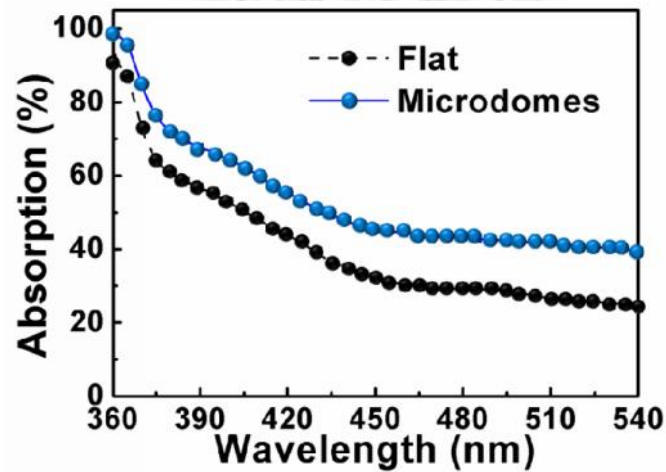
structures.

Figure 4.6 The absorption spectra of InGaN MQW SCs with and without microdome

structures.

§ 4-4   Summary

In conclusion, InGaN MQW SCs with microdome surfaces were fabricated. In comparison with the flat surface, the microdome structures show improved fill factor and J_{sc}, leading to the   enhancement by up to 102 %. The p-GaN microdomes exhibit the enhanced optical absorption due to light trapping effects and possible improvement of photocarrier separation/collection for the MQW SCs due to the strain relaxation, resulting in enhanced EQE and IQE. With the advantages of the simple process and the mechanical robustness, the microdomes grown during SC epitaxial growth offer a viable way to boost solar efficiency of a variety of SCs.
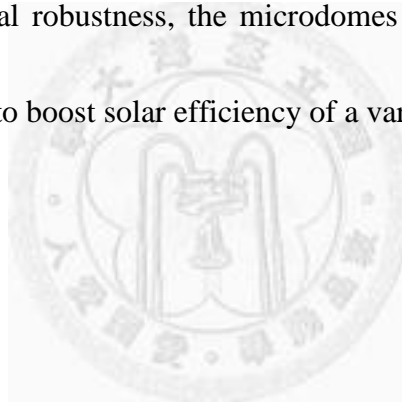
§ 4-5　References

[1] K. Y. Lai, G. J. Lin, Y. L. Lai, Y. F. Chen, and J. H. He, Appl. Phys. Lett. **96**, 81 (2010).

[2] K. Y. Lai, G. J. Lin, C.-Y. Chen, Y.-L. Lai, and J. H. He, IEEE Electron Dev. Lett. **32**, 179 (2011).

[3] G. J. Lin, K. Y. Lai, C. A. Lin, Y.-L. Lai, and J. H. He, IEEE Electron Dev. Lett. **32**, 1104 (2011).

[4] E. Matioli, C. Neufeld, M. Iza, S. C. Cruz, A. A. A. Heji, X. Chen, R. M. Farrell, S. Keller, S. DenBaars, U. Mishra, S. Nakamura, J. Speck, and C. Weisbuch, Appl. Phys. Lett. **98**, 021102 (2011).

[5] T. Fujii, Y. Gao, R. Sharma, E. L. Hu, S. P. DenBaars, and S. Nakamura, Appl. Phys. Lett. **84**, 855 (2004).

[6] P. H. Fu, G. J. Lin, C. H. Ho, C. A. Lin, C. F. Kang, Y. L. Lai, K. Y. Lai, and J. H. He, Appl. Phys. Lett. **100**, 013105 (2012).

[7] G. J. Lin, K. Y. Lai, C. A. Lin, and J. H. He, Opt. Lett. **37**, 61 (2012).

[8] Z. Fan, and J. C. Ho, Int. J. Nanoparticles **4**, 164 (2011).

[9] Y. R. Lin, K. Y. Lai, H. P. Wang, and J. H. He, Nanoscale **2**, 2765 (2010).

[10] Y. R. Lin, H. P. Wang, C. A. Lin, and J. H. He, J. Appl. Phys. **106**, 114310 (2009).

[11] D. S. Tsai, C. A. Lin, W. C. Lien, H. C. Chang, Y. L. Wang, and J. H. He, ACS Nano **5**, 7748 (2011).

[12] J. Q. Xi, M. F. Schubert, J. K. Kim, E. F. Schubert, M. F. Chen, S. Y. Lin, W. Liu, and J. A. Smart, Nature Photonic **1**, 176 (2007).

[13] Y. K. Ee, P. Kumnorkaew, R. A. Arif, H. Tong, H. Zhao, J. F. Gilchrist, and N. Tansu, IEEE J. Sel. Top. Quantum Electron. **15**, 1218 (2009).

[14] P. Kumnorkaew, Y. K. Ee, N. Tansu, and J. F. Gilchrist, Langmuir **24**, 12150 (2008).

[15] X. H. Li, R. Song, Y. K. Ee, P. Kumnorkaew, J. F. Gilchrist, and N. Tansu, IEEE Photonics Journal **3**, 489 (2011).

[16] W. H. Koo, W. Youn, P. Zhu, X. H. Li, N. Tansu, and F. So, Adv. Funct. Mater. DOI: 10.1002/adfm.201200876, (2012).

[17] M. A. Tsai, P. C. Tseng, H. C. Chen, H. C. Kuo, and P. Yu, Opt. Express **19**, A28 (2011).

[18] C. Huh, K. S. Lee, E. J. Kang, and S. J. Park, J. Appl. Phys. **93**, 9383 (2003).

[19] H. M. Kim, Y. H. Cho, H. Lee, S. I. Kim, S. R. Ryu, D. Y. Kim, T. W. Kang, and K. S. Chung, Nano Lett. **4**, 1059 (2004).

[20] Y. H. Sun, Y. W. Cheng, S. C. Wang, Y. Y. Huang, C. H. Chang, S. C. Yang, L. Y. Chen, M. Y. Ke, C. K. Li, Y. R. Wu, and J. J. Huang, IEEE Electron Dev. Lett. **32**, 182 (2011).

[21] M. Y. Ke, C. Y. Wang, L. Y. Chen, H. H. Chen, H. L. Chiang, Y. W. Cheng, M. Y. Hsieh, C. P. Chen, and J. J. Huang, IEEE J. Sel. Top. Quant. **15**, 1242 (2009).

[22] Z. Q. Li, M. Lestradet, Y. G. Xiao, and S. Li, Phys. Status Solidi A **208**, 928 (2011).

[23] H. P. Wang, K. T. Tsai, K. Y. Lai, T. C. Wei, Y. L. Wang, and J. H. He, Opt. Express **20**, A94 (2012).

[24] Y. C. Chao, C. Y. Chen, C. A. Lin, and J. H. He, Energy Environ. Sci. **4**, 3436 (2011).

[25] B. M. Kayes, H. A. Atwater, and N. S. Lewis, J. Appl. Phys. **97**, 114302 (2005).

[26] K. Sun, A. Kargar, N. Park, K. N. Madsen, P. W. Naughton, T. Bright, Y. Jing, and D. Wang, IEEE J. Sel. Top. Quant. **17**, 1033 (2011).

[27] J. J. Wierer, Jr., D. D. Koleske, and S. R. Lee, Appl. Phys. Lett. **100**, 111119 (2012).

Chapter 5   Efficient light harvesting scheme for InGaN-based quantum well solar cells employing the hierarchical structure: SiO$_2$ nanorods/p-GaN microdomes

§ 5-1   Introduction

InGaN-based multiple quantum well (MQW) solar cells (SCs) have a direct and tunable bandgap, which covers nearly the entire solar spectrum. In addition, they also possess advantages as high absorption coefficients, high mobilities, and superior radiation resistance, which allow the operation under harsh environments.[1-3] Employing MQW structures can provide the independent design between the short-circuit current (J_{sc}) and open-circuit voltage (V_{oc}) [4], and also avoid the undesired trade-off between solar response and crystalline quality [4-6]. However, the conversion efficiencies ( ) of InGaN-based SCs are still limited. Methods for either internal quantum efficiency (IQE) or external quantum efficiency (EQE) improvements of SCs have been devoted to boost their photovoltaic (PV) performances.[7-9]

Recently, a variety of subwavelength structures (SWSs) have been demonstrated to effectively suppress the undesired Fresnel reflections. These roughened structures

can be used as the light trapping layer with many superior antireflective (AR) characteristics.[10-13] One efficient AR SWS is the subwavelength nanorod arrays (NRAs) structure, which can be regarded as an intermediate medium with an effective refractive index (n_{eff}) between the air and device surface.[14,15] This leads to the suppressed interface reflection over a wide range of wavelengths due to the effective medium effect.[16] To avoid the abrupt refractive index (n) change at air/device interface, SiO_2 is an attractive candidate AR material due to its intermediate refractive index (n=1.56) between air (n=1) and GaN (n=2.5). Since structuring techniques that require a high-cost lithography process might be a limit to the practical use, a process with the nature lithography is of great interest due to its simplicity and effectiveness. Therefore, SiO_2 NRAs fabricated by simple and photoresist-free techniques are particularly attractive to SC applications.[17]

Besides utilizing the added AR SWSs to improve the performances of InGaN SCs, surface texturing using the structured p-GaN is also under consideration. For examples, it is recently found that InGaN light-emitting diodes (LEDs) with roughened p-GaN structures can effectively enhance light extraction efficiencies by avoiding the severe total internal reflection in device interfaces.[18,19] The texturized p-GaN also leads to improved crystal qualities due to the relaxation of in-plane strain and consequent reduction of piezoelectric field.[20,21] These merits brought by

roughening p-GaN are expected to benefit the PV performances of InGaN SCs, yet the related studies remain scarcely reported to date. Consequently, a hierarchical structure combining the SiO_2 NRAs and roughened p-GaN is worth of studying.

In this letter, we employ the hierarchical structure combined SiO_2 NRAs/p-GaN microdomes to enhance the light harvesting in InGaN MQW SCs. The SiO_2 NRAs are fabricated upon p-GaN microdomes utilizing self-assembled Ag nanoparticles as a mask and reactive ion etching (RIE) techniques with photoresist-free capability. With p-GaN microdomes performed for improving device quality and trapping of light, the added SiO_2 NRAs can further reduce the surface reflections over a wide range of wavelengths. Measurments of PV properties indicate a high fill factor resulted from the p-GaN microdomes and the additionally generated photocurrents came from the excellent light absorption of the hierarchical structure. The corresponding   of the SiO_2 NRA/p-GaN microdome SC exhibits a 1.47-fold enhancement. Simulation results based on finite-difference time-domain (FDTD) analysis prove that the improved PV performances are attributed to the superior optical absorption in the MQW layers upon the application of SiO_2 NRAs/p-GaN microdomes. Design concept and fabrication techniques adopted here provide a viable scheme for light harvesting in nitride-based SCs.

§ 5-2　Experiment

The device preparations here for planar p-GaN and p-GaN microdome SCs were the same as that in chapter 4. To further perform a hierarchical surface, SiO_2 NRAs are fabricated on the microdomed SC surface with the procedures shown in Fig. 5.1: Ag (15 nm)/SiO_2 (450 nm) films were subsequently deposited by electron beam evaporation onto the ITO layer with p-GaN microdomes (Figs. 5.1(a)－(b)). Then, a thermal annealing process was carried out in the furnace at 280℃ for 2 min, leading to segregated Ag nanoparticles through a self-assembly mechanism (Fig. 5.1(c)). Using these Ag nanoparticles as etching masks, the SiO_2 layer was patterned by the reactive ion etching (RIE) process with CHF_3 gas (30 SCCM) and rf power of 90 W for 9 min (Fig. 5.1(d)). After removing the remaining Ag nanoparticles by HNO_3, the vertically aligned SiO_2 NRAs were obtained on the p-GaN microdome layer (Fig. 5.1(e)).
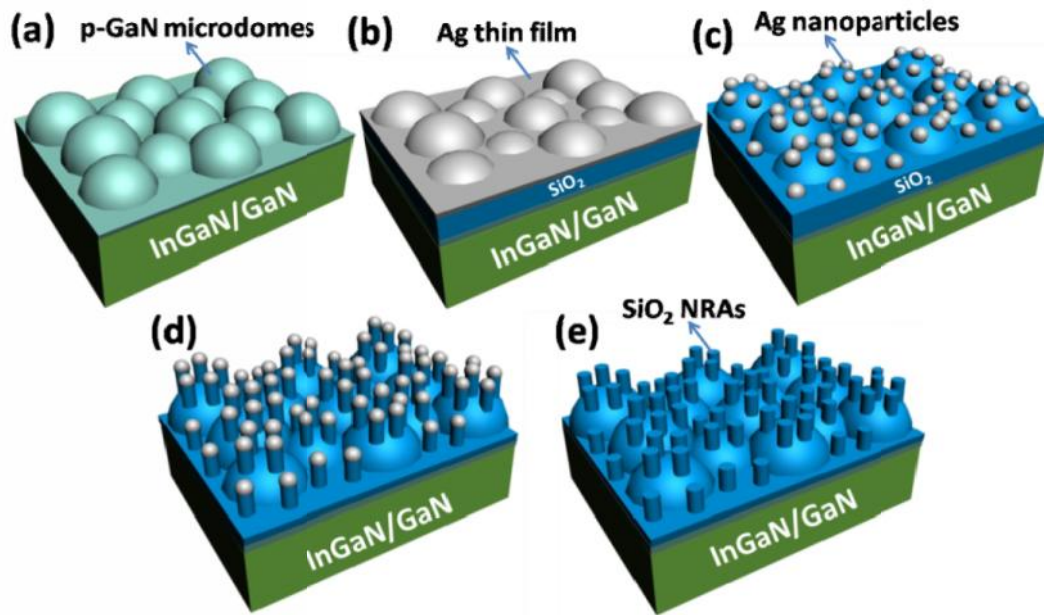
Figure 5.1 Schematic of fabrication procedures for the SiO$_2$ nanorod/p-GaN microdome structure on InGaN/GaN SCs.

§ 5-3 Results and Discussion

Fig. 5.2 shows the SEM images of the p-GaN microdomes and SiO$_2$ NRAs. Fig. 5.2(a) and the inset are the cross-sectional and 45-degree-tilted images of p-GaN microdome SC respectively. The geometric dimensions of these p-GaN microdomes are 530 ± 250 nm in height and 600 ± 370 nm in diameter. Fig. 5.2(b) and the inset are the the cross-sectional and 45-degree-tilted images of the hierarchical SiO$_2$ NRA/p-GaN microdome structure. These vertically aligned SiO$_2$ NRAs are in heights ranging from 300 to 450 nm, and diameters are in 90–180 nm range. Heights and diameters of SiO$_2$ NRAs are controllable through the etching time and the annealing

conditions (duration & temperature) for the Ag thin film. The hierarchical

nano-/micro- structure is found to be dispersively distributed on the SC surface.
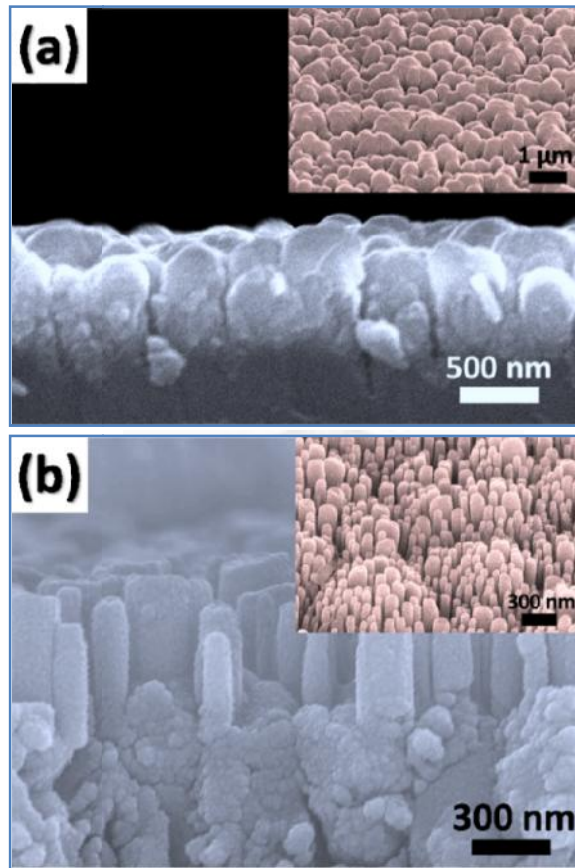
Figure 5.2 (a) and the inset are cross-sectional and 45 degree SEM images of p-GaN
microdome device, respectively. (b) and the inset are cross-sectional and
45 degree SEM images of SiO$_2$ NRA/p-GaN microdome device,
respectively.

Fig. 5.3 presents the specular reflectance measured on three surface conditions

with wavelengths ranging from 340 to 600 nm. It is noted that the SiO$_2$ NRA/p-GaN

microdome structure exhibits the lowest reflectance for all studied wavelengths,

followed by the moderately suppressed values on the bare p-GaN microdome, and the planar p-GaN surface gives the highest reflectance. The results demonstrate that surface reflectance can be effectively mitigated by the presented technique for interface-roughening, and further reduce the undesired Fresnel reflections by roughening the surface from micro-scale to nano-/micro- scale.

The decrement in reflectance for the roughened surfaces can be explained by several effects. Firstly, the p-GaN microdome structure leads to the light trapping effect due to severe light scattering. Inside the microdomes, light diffracts to several beams and re-bounces between the microdomes, which prevents photons from escaping back to air. Microdomes contribute to the trapping of light, and thus result in the decreased reflectance. Condsidering the addition of SiO_2 NRAs, the subwavelength dimensions of NRAs and the low refractive index of SiO_2 make the SiO_2 NRAs behave like an effective medium with an improved impedance match between air and microdomed p-GaN, leading to the destructive interferences between the reflected beams, in which the waves with different phases can partially or wholly cancel one another. Besides, the multiple reflections between the SiO_2 NRAs can also help trap the reflected light. The lowest reflectance achieved by the hierarchical structure manifests the fact that thickening the effective medium induces additional destructive interferences and further suppresses the reflections. As a result, with the

mechanisms of light trapping between the microdomes or NRAs and the effective

medium effect of NRAs, the hierarchical structure provides broadband reduction of

reflectance and thus increases the opportunity of optical absorption by the underneath

material.
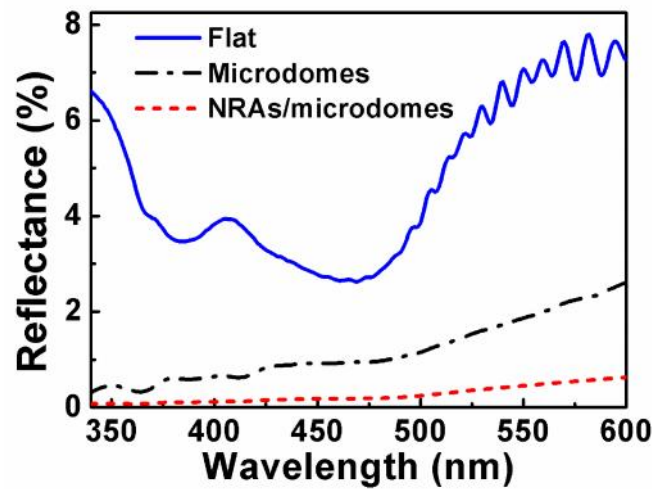
Figure 5.3 Specular reflection measured on the MQW SCs with planar, p-GaN

microdome and SiO_2 NRA/p-GaN microdome surfaces.

In order to study the optical transmission across the different interfaces, the

distributions of electromagnetic fields within the device structures were simulated by

FDTD analysis. We modeled three different geometric features of device surfaces:

planar, p-GaN microdome and SiO_2 NRA/p-GaN microdome, with a 400-nm incident

light. Fig. 5.4(a)–(c) show the transverse electric (TE)-polarized electric field

intensity, $|E_y|$, for the MQW SCs with three surface conditions. One can see that the

field intensities transmitted into the device are mostly enhanced upon the applications of SiO$_2$ NRA/p-GaN microdome surface, as compared with the other two surfaces. One can also notice that fields are strongly confined within the SiO$_2$ NRAs/p-GaN microdomes, indicating the superior light trapping ability of this hierarchical structure. The strong scattering and trapping of light by the nano-/micro- structured surface prolongs the optical path, which is consequently expected to enhance the optical transition across the air/device interface.

The normalized optical absorption, integrated over the MQW region, as a function of times for three different SCs is shown in Fig. 5.4(d). The steady-state absorption values for devices with planar, p-GaN microdomes and SiO$_2$ NRAs/p-GaN microdomes are 0.65, 0.75 and 0.78, respectively. The results indicate that the hierarchical structure not only strengthen the field distribution within the device by increasing the light scattering on the roughened surface but also help light propagate across the interfaces by avoiding the abrupt index transition from air to device. The enhanced optical absorption is expected to benefit efficiencies of the SCs.
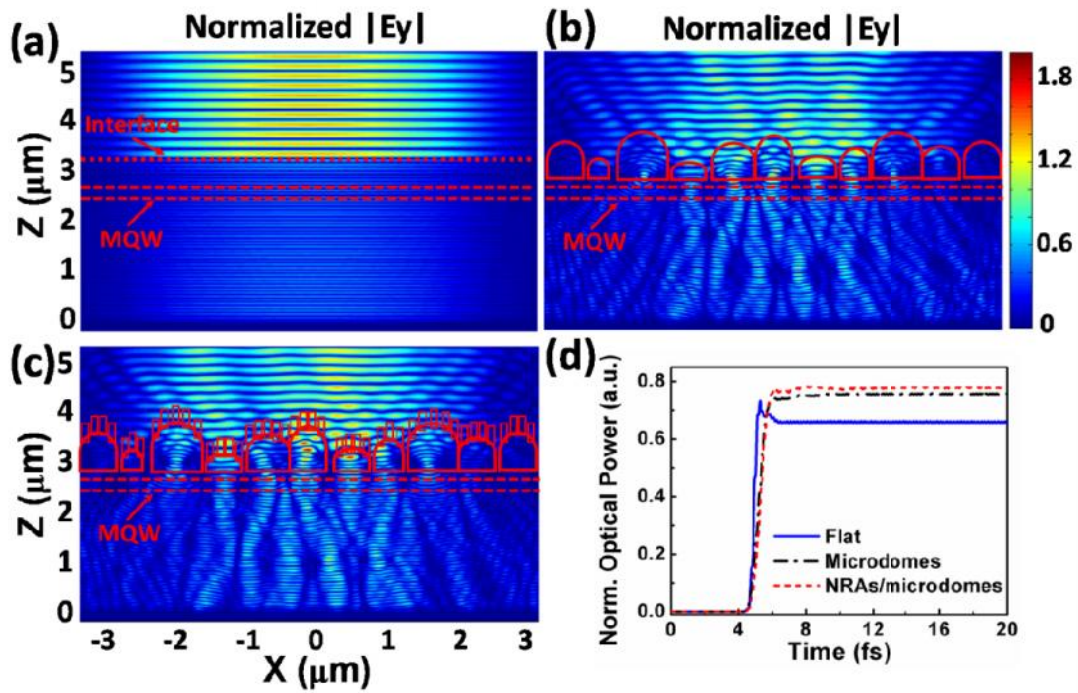
Figure 5.4 Time-averaged and normalized TE electric field distribution, $|Ey|$, simulated by FDTD analysis with different surface structures, (a) Planar, (b) p-GaN microdomes, (c) SiO_2 NRAs/p-GaN microdomes with a 400-nm incident light. (d) Normalized optical power, integrated over the MQW region, as a function of times for the three SCs.

Fig. 5.5(a) shows the measured current density–voltage (J–V) curves of the three SCs. The measured device characteristics are summarized in Table 5.1. In comparison with planar SC, the enhanced J_{sc} and fill factors (FF) for SCs with p-GaN microdomes are respectively due to enhanced light absorption by the microdome surface and the improved device quality caused by the p-GaN roughening[18,20-22]. To gain insight into the device quality, extra IQE measurement is carried out (not shown here) for the microdomed SCs, showing a 1.51-fold enhancement of peak IQE as compared with

43

that of the planar SC. This IQE improvement echoes with the enhanced FF, which may both result from relaxation of in-plane strain and consequent reduction of piezoelectric fields during p-GaN microdome growth.[23] The highest increment in J_{sc} for SiO_2 NRA/p-GaN microdome structure indicates that it further enhances the light absorption of SCs, which agrees with the EQE results. Due to the notable increases in J_{sc} and fill factor, the cell with the hierarchical structure attains the largest   , which is respectively 21 % and 146 % higher than that obtained on bare p-GaN microdome and planar cells. This confirms that the structured surface with SiO_2 NRA/p-GaN microdome can greatly enhances the light absorption of SCs, and thus gives rise to the highest photocurrent. The results prove that it is of great benefit using the hierarchical structure to boost the PV performances of nitride-based SCs.

The EQE spectra for the three cells are shown in Figure 5.5(b), showing the influence of p-GaN microdomes and SiO_2 NRAs on the PV performances. As compared with planar SC, EQEs of the other two SCs with roughened surfaces show improvements at 360–450 nm. The improved light absorption and IQE by the p-GaN microdomes result in the higher EQEs for microdomed SCs. With the added NRAs to the microdomed SCs, the excellent light harvesting of SiO_2 NRAs/p-GaN microdomes leads to the highest EQE. This observation is consistent with the reflection spectra in Fig. 5.2, where it shows that the reflectance on the hierarchical surface is obviously

reduced at the same wavelength range. The results also echo with those revealed by

FDTD analysis.

Table 5.1 Device characteristics of InGaN MQW SCs with three surface structures.

Surface structure	J_{sc} (mA/cm^2)	V_{oc} (V)	FF (%)	(%)
Planar	0.43	2.28	44.1	0.43
p-GaN microdomes	0.54	2.23	72.4	0.87
SiO$_2$ NRAs/p-GaN microdomes	0.67	2.22	72.6	1.06
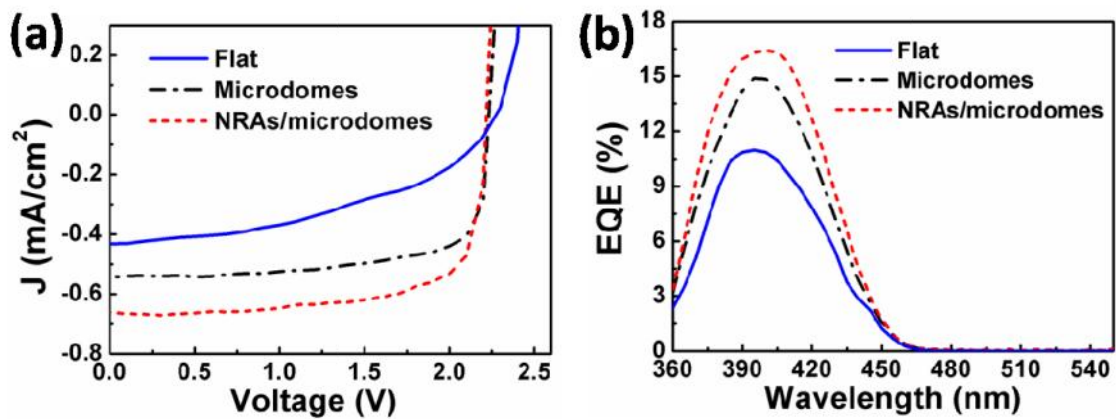
Figure 5.5 (a) *J–V* characteristics and (b) EQE curves measured on the MQW SCs

with three surface conditions.

§ 5-4　Summary

In summary, we performed nano-/micro- scale surface employing SiO_2 NRAs/p-GaN microdomes to enhance the light harvesting on InGaN MQW SCs. The hierarchical structure significantly suppresses specular reflections over a wide range of wavelengths, which is attributed to light trapping effects of microdomes or NRAs and the effective medium effect of NRAs. Compared with planar and p-GaN microdome structures, the SiO_2 NRA/p-GaN microdome structure showed the best PV performances. The increments of EQE and fill factor contributed to the giant enhancement by up to 146 % and 21 %, as compared with planar and bare microdome surfaces respectively. The presented light harvesting scheme using the hierarchical structure demonstrates a feasible efficiency-boosting scheme for a wide variety of PV devices.

§ 5-5　References

[1]　J. Wu, W. Walukiewicz, K. M. Yu, J. W. Ager, E. E. Haller, H. Lu, W. J. Schaff, *Appl. Phys. Lett.* **2002**, *80*, 4741.

[2]　J. Wu, W. Walukiewicz, K. M. Yu, W. Shan, J. W. Ager, E. E. Haller, H. Lu, W. J. Schaff, W. K. Metzger, S. Kurtz, *J. Appl. Phys.* **2003**, *94*, 6477.

[3]　R. Dahal, B. Pantha, J. Li, J. Y. Lin, H. X. Jiang, *Appl. Phys. Lett.* **2009**, *94*, 063505.

[4]　K. W. J. Barnham, G. Duggan, *J. Appl. Phys.* **1990**, *67*, 3490.

[5]　K. Y. Lai, G. J. Lin, Y. L. Lai, Y. F. Chen, J. H. He, *Appl. Phys. Lett.* **2010**, *96*, 081103.

[6]　K. Y. Lai, G. J. Lin, Y. L. Lai, J. H. He, *IEEE Electron Dev. Lett.* **2011**, *32*, 179.

[7]　D. Hofstetter, E. Baumanna, F. R. Giorgettaa, M. Maierb, F. Guillotc, E. Bellet-Amalricc, E. Monroy, *Appl. Phys. Lett.* **2006**, *88*, 121112.

[8]　C. L. Chao, C. H. Chiu, Y. J. Lee, H. C. Kuo, P. C. Liu, J. D. Tsay, S. J. Cheng, *Appl. Phys. Lett.* **2009**, *95*, 051905.

[9]　P. H. Fu, G. J. Lin, C. H. Ho, C. A. Lin, C. F. Kang, Y. L. Lai, K. Y. Lai, J. H. He, *Appl. Phys. Lett.* **2012**, *100*, 013105.

[10]　Z. Y. Fan, D. J. Ruebusch, A. A. Rathore, R. Kapadia, O. Ergen, P. W. Leu, A. Javey, *Nano Res.* **2009**, *2*, 829.

[11]　J. Zhu, Z. Yu, G. F. Burkhard, C.-M. Hsu, S. T. Connor, Y. Xu, Q. Wang, M. McGehee, S. Fan, Y. Cui, *Nano Lett.* **2009**, *9*, 279.

[12]　Y. A. Dai, H. C. Chang, K. Y. Lai, C. A. Lin, R. J. Chung, G. R. Lin, J. H. He, *J. Mater. Chem.* **2010,** *20*, 10924.

[13]　H. C. Chang, K. Y. Lai, Y. A. Dai, H. H. Wang, C. A. Lin, J. H. He, *Energy Environ. Sci.* **2011**, *4*, 2863.

[14] Y. C. Chao, C. Y. Chen, C. A. Lin, Y. A. Dai, J. H. He, *J. Mater. Chem.* **2010**, *20*, 8134.

[15] K. Y. Lai, Y. R. Lin, H. P. Wang, J. H. He, *Cryst. Eng. Comm.* **2011**, *13*, 1014.

[16] Y. R. Lin, K. Y. Lai, H. P. Wang, J. H. He, *Nanoscale* **2010**, *2*, 2765.

[17] J. H. Hsieh, Chuan Li, Y. Y. Wub, S. C. Jang, *Curr. Appl. Phys.* **2010**, *11*, S328.

[18] C. F. Lin, J. H. Zheng, Z. J. Yang, J. J. Dai, *Appl. Phys. Lett.* **2006**, *88*, 083121.

[19] P. C. Tsai, W. R. Chen, Y. K. Su, C. Y. Huang, *Appl. Surf. Sci.* **2010**, *256*, 6694.

[20] Y. H. Sun, Y. W. Cheng, S. C. Wang, Y. Y. Huang, C. H. Chang, S. C. Yang, L. Y. Chen, M. Y. Ke, C. K. Li, Y. R. Wu, J. J. Huang, *IEEE Electron Dev. Lett.* **2011**, *32*, 182.

[21] M. Y. Ke, C. Y. Wang, L. Y. Chen, H. H. Chen, H. L. Chiang, Y. W. Cheng, M. Y. Hsieh, C. P. Chen, J. J. Huang, *IEEE J. Sel. Top. Quant.* **2009**, *15*, 1242.

[22] C. Huh, K. S. Lee, E. J. Kang and S. J. Park, *J. Appl. Phys.* **2003**, *93*, 9383.

[23] Z. Q. Li, M. Lestradet, Y. G. Xiao and S. Li, *Phys. Status Solidi A* **2011**, *208*, 928.

Chapter 6   Light emission enhancement of GaN-based light-emitting diodes via the hierarchical structure: SiO$_2$ nanorods/p-GaN microdomes

§ 6-1   Introduction

Nitride-based light emitting diodes (LEDs) have been utilized in various applications, such as displays, cell phones, and general lighting.[1] The huge commercial success is the main driving force of the intensive research efforts in this field. As the internal quantum efficiencies (IQE) of InGaN-based quantum wells have been well above 60% due to the advance of epitaxial growth technologies, the external quantum efficiencies (EQE), being mostly below 50%, are still in need of effective approaches for further improvement. One of the hurdles to be overcome is the large difference in refractive index (n) between the air (n=1) and GaN (n~2.5) [2], leading to a very limited critical angle, $_c$~23°, for light escape from the air/semiconductor interface. Numerous studies on light extraction enhancement of GaN LEDs had been reported.[3-5] Surface roughening is among the popular methods. Roughening GaN surface via wet or dry etching technologies has recently been reported.[6-8] It is demonstrated that the textured surfaces can result in enhanced light trapping by the scattering effects on the roughened surface. Furthermore, IQE of

LEDs can also be improved by the texturing of p-GaN, which is due to the relaxation of in-plane strain and consequent reduction of piezoelectric field.[9,10]

Moreover, a variety of nanostructures have been introduced to avoid the abrupt change of refractive index at air/device interface to reduce the interface reflection, leading to improved light extraction/harvesting efficiency. For examples, the improved light-harvesting of solar cells can be realized using nanostructures as ZnO nanorods [11-13], Si nanowires [14], SiO_2 nano-honeycombs [15], etc. On the other hand, the light emission intensity of GaN LEDs can be enhanced via ZnO nanorods [16-19], micropillars [20] and pyramid structures [21,22] due to the improved light extraction. Among the materials for light-harvesting nanostructures, SiO_2 is a promising candidate due to its intermediate refractive index (n~1.55 at 460 nm) [23] between air and GaN, the low absorption in visible region [24,25], and the wide bandgap of 8.9 eV [25], which is well above the emission energies of nitride-based LEDs. As Yik Khoon *et al.* reported [26], SiO_2 nanostructures obtained by the fabrication with photoresist-free and wafer-scale-uniformity capabilities are particularly applicable to photon extraction from LEDs. Besides, it is recently found that SiO_2 nanostructures can be produced by a nature lithography technique utilizing simple annealing process.[27] Therefore, SiO_2 nanorods arrays (NRAs) produced by a self-assembled Ag nanoparticles and dry etching method hold a great promise for

solid-state lighting, and yet relevant studies has been scarcely reported. It is worth to

be mentioned that hierarchical structures integrating nano- and micro-scale roughness

usually present superior and unique functionalities, which are expected to bring

additional advantages beyond single structures.[28,29] For example, the hierarchical

ZnO NRA/silica microsphere structure is investigated to have large light scattering

efficiency due to the further light-scattering enhancement by ZnO NRAs.[30] The

reported nano-/micro- structure is a promising candidate for photovoltaic and

optoelectronic device applications.

In this study, we fabricated the hierarchical SiO_2 NRA/p-GaN microdome

structure on GaN-based LEDs, in order to improve the light extraction efficiencies.

Bare p-GaN microdomes are regarded as scattering centers, which help enhance the

LED light output by 16.7 % at 20 mA. Upon the microdomes, the added SiO_2 NRAs

can further reduce the internal total reflections by mitigating the index change of

air/GaN interface. LEDs employing the hierarchical structure exhibit an excellent

improvement of output intensity by up to 36.8 %, which is attributed to the efficient

scattering effect on the surface texture and the improved impedance match between

air and GaN. Finite-difference time-domain (FDTD) simulations solving Maxwell's

equations are performed to simulate the light propagation across the nanostructure

interfaces. The results show that the hierarchical surface structure leads to additional

photons escaping from the air/device interface, and thus results in the enhanced light extraction. The proposed concept in this study should benefit the development of nitride-based LEDs and many other optoelectronic devices.

§ 6-2   Experiment

The MQW blue LEDs were grown by metal–organic chemical vapor deposition on c-plane sapphire substrates. The layer structures consist of fifteen periods of intentionally undoped $In_{0.15}Ga_{0.85}N$ (2.4 nm)/GaN (14 nm) MQWs, sandwiched by a 2.5-µm n-type (Si-doped) and a 0.2-µm p-type (Mg-doped) GaN layer. The free carrier concentrations for n-type and p-type GaN are around 2×10^{18} cm^{-3} and 5×10^{17} cm^{-3}, respectively. Ammonia (NH_3), trimethylgallium (TMG, for n-GaN and p-GaN), triethylgallium (TEG, for MQWs), and trimethylindium (TMI) were used as the precursors. Surface morphologies of p-GaN were controlled by TMGa flows and substrate temperatures. For flat p-GaN, TMGa flow rate was 45 µmol/min and substrate temperature was in the range of 950-1100 °C; for p-GaN microdomes, TMGa flow rate was increased to more than 55 µmol/min and substrate temperature was decreased to lower than 920 °C. In device fabrication, indium tin oxide (ITO) was deposited by electron beam evaporation on p-GaN to form transparent ohmic contacts. The 1×1 mm^2 diode mesas were then defined by chlorine-based plasma

etching. The contacting scheme consists of fingered Ti/Al/Ni/Au metal grids with the thicknesses of 20/400/20/2000 nm deposited on the ITO and n-GaN. To fabricate a hierarchical structure, SiO$_2$ NRAs were performed on the p-GaN microdome LED via the same procedures in chapter 5 (see Fig. 5.1).

§ 6-3   Results and Discussion

Fig. 6.1(a) and the inset are respectively the 45-degree-tilted and the cross-sectional SEM images of p-GaN microdome surface. The geometric dimensions of these p-GaN microdomes are 530 ± 250 nm in height and 600 ± 370 nm in diameter. Fig. 6.1(b) and the inset are the 45-degree-tilted and the cross-sectional images of SiO$_2$ NRA/p-GaN microdome surface, respectively. These vertically aligned SiO$_2$ NRAs are around 400 nm high and the diameters range from 50 to 150 nm.
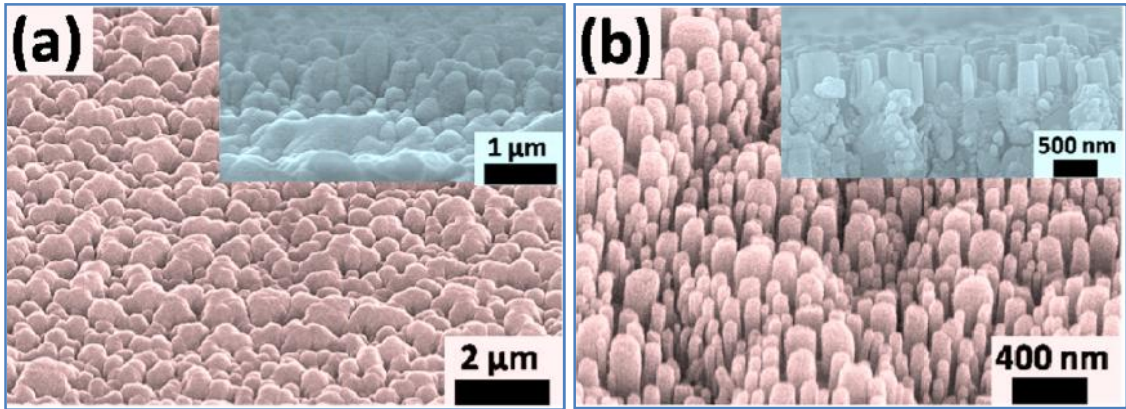
Figure 6.1 (a) and the inset are 45-degree tilted and cross-sectional surface images of p-GaN microdome LED respectively. (b) and the inset are 45-degree tilted and cross-sectional surface images of SiO_2 NRA/p-GaN microdome LED respectively.

The electrical characteristics ($I-V$ curves) of the LEDs are presented in the inset of Fig. 6.2. The devices with p-GaN microdomes and SiO_2 NRAs/p-GaN microdomes respectively show the forward voltages of 3.17 V and 3.21 V at the driving current of 20 mA, which are slightly smaller than that (3.23 V) of the flat device. The result is attributed to the improved ohmic contact resistance due to the increased contact area of microdomed surfaces. Furthermore, the slightly higher operation voltage of NRA/microdome LED than bare microdome LED is attributed to the additional increased series resistances, which are possibly caused by the additional surface recombination centers and damage occurring during the RIE process of SiO_2 NRAs.

Fig. 6.2 shows the light intensity as a function of injection current ($L-I$ curve) for

the three devices. The LED with SiO_2 NRA/p-GaN microdome structure exhibits the highest emission intensities in the entire current range, which is believed to result from the enhanced scattering effects on the hierarchical structure and the smoothened transition of refractive index from GaN to air provided by the SiO_2 NRAs [31-33], both of which greatly improve light extraction from the device.

Compared with flat LED, the emission intensities of bare microdome LED and hierarchical LED exhibit the enhancements of 16.7 % and 36.8 % at 20 mA, respectively. The enhancements of the two textured surfaces are attributed to the improved light extraction or EQE caused by the roughened morphologies. Surface roughening with p-GaN microdomes not only increases the total emission area but also increases the variation of the optical incident angles at the interfaces between GaN and air, which is believed to reduce the undesired total internal reflections within GaN. Besides the enhancement of light extraction efficiency, the p-GaN roughening can further improve the IQE of LEDs which has recently been disscussed.[3,9,34] Accordingly, it is believed that the microdomed p-GaN can increase the LED light output due to the improved light extraction and IQE. For the hierarchical structure, the added SiO_2 NRAs can be regarded as an intermediate medium with the gradient refractive index further mitigating the abrupt index change between air and p-GaN microdomes. This effective medium effect additionally suppresses the Fresnel

reflections from device to air. Consequently, the hierarchical structure results in the

most light extraction of LEDs.
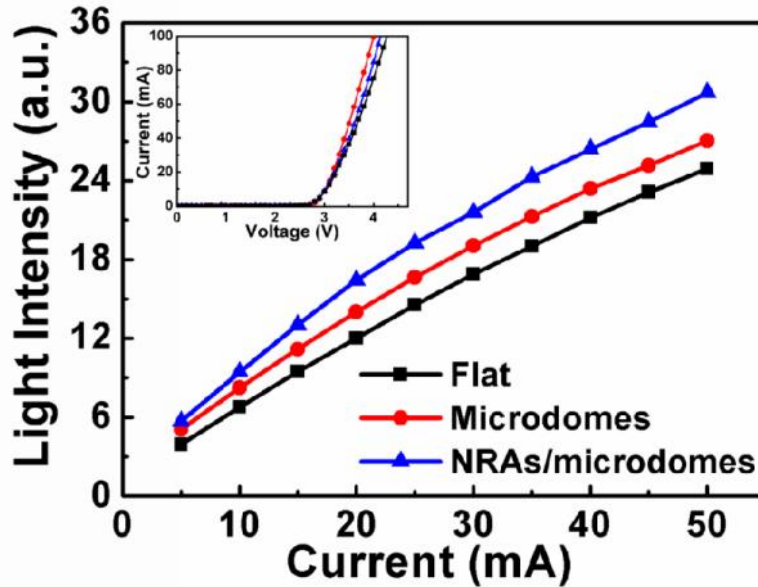
Figure 6.2 Light-output intensity versus injection currents ($L-I$ curves) of flat,
p-GaN microdome, and SiO_2 NRA/p-GaN microdome LEDs. The inset is
the corresponding $I-V$ characteristics.

In order to reveal the light propagation across the roughened surface structures,

the distributions of electromagnetic fields within the device structures were simulated

by FDTD analysis. We modeled three different geometric features of the LEDs with

flat, p-GaN microdome, and SiO_2 NRA/p-GaN microdome surfaces. Fig. 6.3(a)−(c)

visualize the time-averaged TE-polarized electric field intensity distributions, $|E_y|$, for

GaN blue LEDs with different surface conditions at 460 nm wavelength. All of the

calculated values are normalized to the ones of the excitation source. It can be seen that the emitted field intensities (in air) of both p-GaN microdome and SiO_2 NRA/p-GaN microdome devices are enhanced. Compared with the flat LED of Fig. 6.3(a), the p-GaN microdome structure, marked in Fig. 6.3(b), results in strong field intensities on the roughened surface, indicating enhanced light scattering. Moreover, in Fig. 6.3(c), one can see that the regions of SiO_2 NRAs/p-GaN microdomes further strengthen field intensities inside the microdomes and NRAs, and lead to the most scattering centers on the device surface. The strong scattering and re-bouncing of light within SiO_2 NRAs/p-GaN microdomes signal an improved light extraction from the device internal, which are supported by the observation that the light trapped inside the device in Fig. 6.3(c) is less than that in Fig. 6.3(b) and this results in less field intensity leaking out from the backside (through n-GaN and sapphire). In other words, integrating SiO_2 NRAs with p-GaN microdomes not only help light propagate across the interfaces by avoiding the abrupt index transition from GaN to air but also reinforce the field distribution within the roughness by increasing the light scattering through the surfaces. As a result, this hierarchical structure leads to the most light extraction.

Fig. 6.3(d) shows the normalized optical power, integrated over the marked regions, as a function of time for the three LEDs. Steady-state power values for the

three devices are 0.647, 0.693 and 0.791, respectively. Compared with the flat LED, the optical power enhancement of the two textured LEDs are 7.1 % and 22.3 %, respectively. This indicates that these textured nanostructures can increase the number of the photons leaving LEDs, and thus enhance light extraction efficiency.
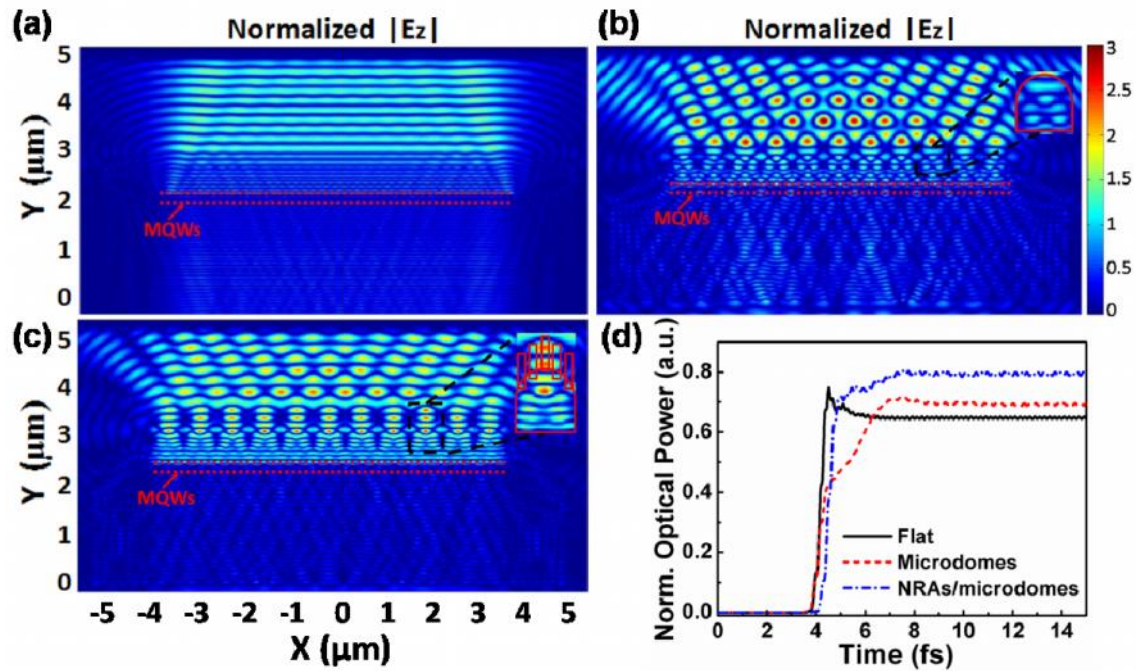
Figure 6.3 Time-averaged and normalized TE electric field distribution, $|E_y|$, simulated by FDTD analysis with different surface conditions at 460 nm wavelength, (a) Flat, (b) p-GaN microdome, (c) SiO$_2$ NRA/p-GaN microdome, (d) Normalized optical power, integrated over the framed regions, as a function of times for the three LEDs.

Fig. 6.4 indicates the normalized radiation profiles of the three LED samples. The

corresponding viewing angles of flat, microdome, and NRA/microdome LEDs are

112˚, 114˚ and 115˚, respectively. The wider and stronger emission cone of

NRAs/microdomes LEDs is in line with the enhanced scattering effects shown in Fig.

6.3(c), confirming the excellent scattering and light-extraction abilities of the

NRAs/microdomes [16]. This lambertian light emission might be beneficial to the

applications in general lighting.
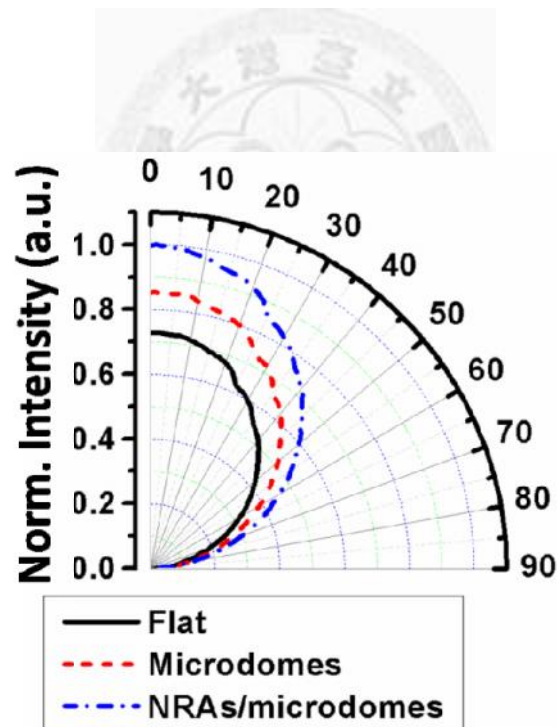
Figure 6.4 Radiation patterns of the three LEDs under a 20 mA injected current.

§ 6-4　Summary

In summary, we fabricated two surface-textured LEDs respectively with p-GaN microdomes and SiO_2 NRAs/p-GaN microdomes. Using self-assembled Ag nanoparticles as etching masks and subsequent RIE, the fabricated SiO_2 NRA/p-GaN microdome LED enhances light output intensity at 20 mA by up to 36.8 %, as compared with flat LED. The SiO_2 NRAs provide an effective refraction index to reduce the total internal reflection at the air/GaN interface and the microdomes lead to stronger light scattering effect, increasing the light extraction efficiency of LEDs. The presented concept and manufacturing technique of surface roughening would be a viable way to enhance the light extraction efficiency for nitride-based LEDs.
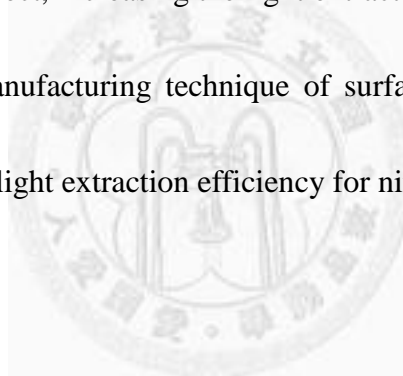
§ 6-5 References

[1] C. C. Sun, I. Moreno, S. H. Chung, W. T. Chien, C. T. Hsieh, and T. H. Yang, *J. Soc. Inf. Display* **2008**, *16*, 519.

[2] R. Goldhahn, J. Scheiner, S. Shokhovets, T. Frey, U. Khler, D. J. As, and K. Lischka, *Appl. Phys. Lett.* **2000**, *76*, 291.

[3] M. Y. Ke, C. Y. Wang, L. Y. Chen, H. H. Chen, H. L. Chiang, Y. W. Cheng, M. Y. Hsieh, C. P. Chen, and J. J. Huang, *IEEE J. Sel. Top. Quant.* **2009**, *15*, 1242.

[4] T. H. Seo, T. S. Oh, Y. S. Lee, H. Jeong, J. D. Kim, H. Kim, A. H. Park, K. J. Lee, C. H. Hong, and E. K. Suh, *Jpn. J. Appl. Phys.* **2010**, *49*, 092101.

[5] S. J. Tu, J. K. Sheu, M. L. Lee, C. C. Yang, and W. C. Lai, *Opt. Express* **2011**, *19*, 12719.

[6] T. Fujii, Y. Gao, R. Sharma, E. L. Hu, S. P. DenBaars, and S. Nakamura, *Appl. Phys. Lett.* **2004**, *84*, 855.

[7] C. B. Soh, B. Wang, S. J. Chua, Vivian K. X. Lin, Rayson J. N. Tan, and S. Tripathy, *Nanotechnology* **2008**, *19*, 405303.

[8] S. Chhajed, W. Lee, J. Cho, E. F. Schubert, and J. K. Kim, *Appl. Phys. Lett.* **2011**, *98*, 071102.

[9] H. Sun, Y. W. Cheng, S. C. Wang, Y. Y. Huang, C. H. Chang, S. C. Yang, L. Y. Chen, M. Y. Ke, C. K. Li, Y. R. Wu, and J. J. Huang, *IEEE Electron Dev. Lett.* **2011**, *32*, 182.

[10] M. Y. Ke, C. Y. Wang, L. Y. Chen, H. H. Chen, H. L. Chiang, Y. W. Cheng, M. Y. Hsieh, C. P. Chen, and J. J. Huang, *IEEE J. Sel. Top. Quant.* **2009**, *15*, 1242.

[11] G. J. Lin, K. Y. Lai, C. A. Lin, and J. H. He, *Opt. Lett.* **2012**, *37*, 61.

[12] L. K. Yeh, K. Y. Lai, G. J. Lin, P. H. Fu, H. C. Chang, C. A. Lin, and J. H. He, *Adv. Energy Mater.* **2011**, *1*, 506.

[13] G. J. Lin, K. Y. Lai, C. A. Lin, Y.-L. Lai, and J. H. He, *IEEE Electron Dev. Lett.* **2011**, *32*, 1104.

[14] H. C. Chang, K. Y. Lai, Y. A. Dai, H. H. Wang, C. A. Lin, and J. H. He, *Energy Environ. Sci.* **2011**, *4*, 2863.

[15] P. H. Fu, G. J. Lin, C. H. Ho, C. A. Lin, C. F. Kang, Y. L. Lai, K. Y. Lai, and J. H. He, *Appl. Phys. Lett.* **2012**, *100*, 013105.

[16] M. K. Lee, C. L. Ho, and P. C. Chen, *IEEE Photonics Technol. Lett.* **2008**, *20*, 252.

[17] M. K. Lee, C. L. Ho, C. C. Lin, N. R. Cheng, M. H. Houng, Y. K. Chien, and C. F. Yen, *J. Electrochem. Soc.* **2011**, *158*, D286.

[18] S. J. An, J. H. Chae, G. C. Yi, and G. H. Park, *Appl. Phys. Lett.* **2008**, *92*, 121108.

[19] K. K. Kim, S. D. Lee, H. Kim, J. C. Park, S. N. Lee, *Appl. Phys. Lett.* **2009**, 94, 071118.

[20] J. K. Kim, A. N. Noemaun, F. W. Mont, D. Meyaard, E. F. Schubert, D. J. Poxson, H. Kim, C. Sone, and Y. Park, *Appl. Phys. Lett.* **2008**, *93*, 221111.

[21] C. C. Sun, C. Y. Lin, T. X. Lee, T. H. Yang, *Opt. Eng.* **2004**, *43*, 1700.

[22] T. X. Lee, K. F. Gao, W. T. Chien, and C. C. Sun, *Opt. Express* **2007**, *15*, 6670.

[23] E. D. Palik, "Handbook of Optical Constants of Solids," Academic Press.

[24] K. Nakagawa, H. Mikami, T. Ishikawa, Y. Shiraishi, A. Ejiri, H. Matsumoto, and S. Matsumoto, *UVSOR Act Rep* **2005**, *2004*, 88.

[25] R. B. Laughlin, *Phys. Rev. B* **1980**, *22*, 3021.

[26] Y. K. Ee, R. A. Arif, and N. Tansu, *Appl. Phys. Lett.* **2007**, *91*, 221107.

[27] J. H. Hsieh, Chuan Li, Y. Y. Wu, S. C. Jang, *Curr. Appl. Phys.* **2011**, *11*, S328.

[28] X. S. Fang, Y. H. Bando, C. H. Ye, G. H. Shen, D. Golberg, *J. Phys. Chem. C*

2007, *111*, 8469.

[29] H. J. Xu, L. Su, Y. F. Chan, and X. M. Sun, *J. Mater. Res.* **2011**, *26*, 1174.

[30] Y. H. Ko, and J. S. Yu, *Opt. Express* **2011**, *19*, 25935

[31] J. Q. Xi, J. K. Kim, and E. F. Schubert, *Nano Lett.* **2005**, *5*, 1385.

[32] J. Q. Xi, J. K. Kim, E. F. Schubert, Dexian Ye, T. M. Lu, and S. Yu Lin, *Opt. Lett.* **2006**, *31*, 601.

[33] P. Wang, Z. Gan, S. Liu, *Opt. Laser Technol.* **2009**, *41*, 823.

[34] H. C. Wang, T. Y. Tang, C. C. Yang, T. Malinauskas, and K. Jarasiunas, *Thin Solid Films* **2010**, *519*, 863.

Chapter 7   Conclusion

This thesis focuses on the improvements of energy-harvesting for III-V based opticelectronic devices. The former part of the thesis provides insights into the improved-efficiency GaN-based solar cells via nano- and micro- scale AR structures. The latter part focuses on luminance enhancements of GaN-based light-emitting diodes via surface roughening.

In chapter 3, using self-assembled Ag nanoparticles as an etching mask and RIE method, we fabricated low-cost light-trapping SiO_2 NRAs to improve the optical absorption of SCs. This AR layer suppresses the surface reflection via the light trapping effect and the graded n_{eff}, and consequently improves SC conversion efficiency by ~21 %.

In chapter 4, SCs with microdome surfaces were grown, showing improved fill factor and J_{sc}, and   enhancement of 102 %. The p-GaN microdomes exhibit the enhanced optical absorption due to light trapping effects and possible improvement of photocarrier separation/collection for the MQW SCs due to the strain relaxation, resulting in enhanced EQE and IQE.

In chapter 5, the nano-/micro- scale surface with NRAs/microdomes was employed to further enhance the light harvesting on SCs. This hierarchical structure

shows the best PV performances, attributed to light trapping effects of NRAs/microdomes and the effective medium effect of NRAs. The increments of EQE and fill factor contributed to the   enhancement of 146 %, as compared with planar surface.

In chapter 6, GaN blue LED with SiO_2 NRAs/p-GaN microdomes was discussed. The p-GaN microdomes lead to stronger light scattering effect and SiO_2 NRAs provide an effective refraction index to reduce the total internal reflection at the air/GaN interface, increasing the LED light extraction. The two-step roughening helps enhance LED light output by 36.8 % at 20 mA.

To summarize this thesis, we executed a hierarchical structure with nano-/micro-scale roughness, which is both applicable to GaN-based LEDs and SCs. This SiO_2 NRA/p-GaN microdome scheme is not only effective in light extraction for LEDs, but also an efficient light-harvesting layer for SCs.
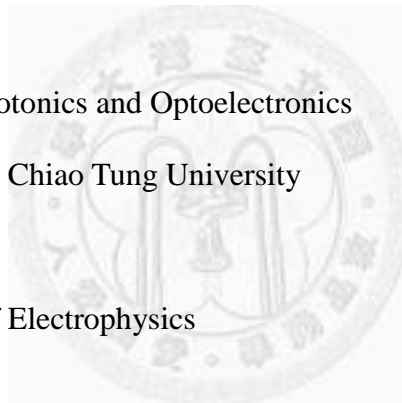
CV

Cheng-Han Ho

何政翰

Personal Details

◆ Date of Birth : Mar. 19, 1988

◆ Nationality : Taiwan

Education

◆ 2010-2012   National Taiwan University

Degree: Master

Major: Institute of Photonics and Optoelectronics

◆ 2006-2010   National Chiao Tung University

Degree: Bachelor

Major: Department of Electrophysics

Research Interest

◆ Optical property and simulation of nanostructures

◆ Synthesis and characterization of SiO_2 nanorod arrays.

◆ Synthesis and characterization of group III-V devices

◆ GaN-based light emitting diodes

◆ InGaN-based solar cells

Publication List

Journal Paper

1. P. H. Fu, G. J. Lin, **<u>C. H. Ho</u>**, C. A. Lin, C. F. Kang, Y. L. Lai, K. Y. Lai, and J. H. He, "Efficiency enhancement of InGaN multi-quantum-well solar cells via light-harvesting SiO_2 nano-honeycombs", *Appl. Phys. Lett.* 100, 013105 (2012) (IF:3.820, 14/116 in Phys., Appl.)(selected for the January 16, 2012 issue of Virtual Journal of Nanoscale Science & Technology)(featured in Semiconductor Today, January (2012))

2. **<u>C.H. Ho</u>**, G.J. Lin, P.H. Fu, C.A. Lin, P.C. Yang, K.Y. Lai and J.H. He[*], "An efficient light-harvesting scheme using Si_{O2} nanorods for InGaN multiple quantum well solar cells", *Sol. Ener. Mater. Sol. Cells*, 103, 194-198 (2012) (IF:4.746, 7/79 in ENERGY & FUELS)

3. **<u>C.H. Ho</u>**, K.Y. Lai, C.A. Lin, M.K. Hsing, and J.H. He*, "Microdome InGaN-Based Multiple Quantum Well Solar Cells", *Appl. Phys. Lett.* 101, 023902 (2012) (DOI: 10.1063/1.4734380)

Press report

1. Guan-Jhong Lin, **<u>Cheng-Han Ho</u>**, Po-Han Fu, Jr-Hau He and Kun-Yu Lai, "Nanorod photon management in nitride-based devices", Dec. 14, 2011, *SPIE Newsroom*, DOI: 10.1117/2.1201112.004008

中文期刊:

1. 賴昆佑、林冠中、**何政翰**、傅柏翰、何志浩，電子資訊期刊-太陽能專刊_
第十七卷第一期_"氮化物太陽能電池".(已刊出)

2. **何政翰** *et al.*，電子材料_第九章: 太陽能電池.(付印中)

Conference Papers

1. P. H. Fu, G. J. Lin, **C. H. Ho**, C.A. Lin, K. Y. Lai, and J. H. He, "Efficiency enhancement of InGaN multi-quantum-well solar cells via antireflective SiO2 nano-honeycombs", *SPIE Photonics West*, San Francisco, USA, 2012.

Patent (ROC)

1. **Cheng-Han Ho**, Guan-Jhong Lin,Kun-Yu Lai,and Jr-Hau He,"奈米粗化陣列結構之製造方法(Method for Manufacturing Nano Roughing Array Structure)"(Submitted)

2. **Cheng-Han Ho**, and Jr-Hau He,"具有微米鐘粗化陣列結構之三五族太陽能電池及其製造方法(III-V Based Solar Cells having Roughened Microdome Array Structure and Manufacturing Method for the Same)"(Applying)